Response to referee comments RC1 Solid Earth se-2018-81

The authors gratefully acknowledge the critical and constructive comments by the referee. In the following, we respond to each of the points raised. The *comments by the referee are given in cursive characters*, our response in blue and the specific changes in the revised manuscript in red. You will find an annotated pdf-file of our revised manuscript below, in which all changes are correlated to the reviewer's comments.

General comment: Particular, the relationship between cracking and recrystallization or low temperature plasticity and recrystallization as presented in the text contain some virtually contradictory or at least inconsistent statements.

As the sequence of associated microcracking and dislocation glide of albite (low-temperature plasticity) followed by growth (by strain-induced grain boundary migration and formation of albite growth rims resulting in a SPO) is one of the major points of this study. We phrased this sequence more carefully, especially in the rewritten chapter 5.6., to avoid misunderstandings (see comment to points 32, 35).

1. Abstract, line 10: Better: "…replacement is interpreted to take place by…"

We changed this accordingly.

line 10: Better: "chemical metastability" instead of "solubility difference", as that term is more general

As formation of these microstructures involve dissolution-precipitation processes, we decided to keep the term "solubility difference", see point 29.

2. Line 11: omit "in contrast"

We omitted "in contrast".

3. line 15: "dislocation glide and strain-induced grain boundary migration" – see general comments and comments below concerning this term

See general comment and response to points 32 and 35.

4. p.3, line 16: Fig. 1 e,g do not exist, only Fig. 1

This was a typesetting error, the e.g. introduces the cited references: (Fig. 1; e.g., Hofmann et al.,1983; …), it is now corrected.

5. p.3, line 28: What is the connection of tertiary ages with the rest of this text?

Tertiary ages are mentionedinthe geologic context. They reveal that the rocks north of the DAV were deformed during alpine metamorphism, in contrast to rocks south of the DAV.

6. p.4, line 11: insert commas after "argued" and "studies"

We added the commas.

7. p.4, line 14: insert "and" after comma

We inserted "and" after comma.

8. p.4, line 15. "mineral" instead of "mineralogical"

We changed this accordingly.

9. p.5, line 10: Are the grain sizes given as diameters of equivalent spheres or circles? Mean or mode of the grain size distribution? Please state more details of the grain size analysis.

We were referring to the diameter of a circle with equivalent diameter. Wenow describethe area normalized grain size as requested by referee#2 (see comments to RC2, point 12).

We describe the grain size analysis in more detail in the chapter methods revised manuscript. "Grain size analysis was by area normalization excluding border grains. The mean and median of the area distribution are given."

10. p.5, line 16: omit the sentence: "Feldspar…". This is a repetition, the situation is better explained below in the text.

We omitted this sentence in the revised text.

11. p.5, line 17: better: "…and rarely shows perthitic…"

We rephrased this sentence accordingly.

12. p.5, line 18: better: "…with Ab95-86 is present and in these grains zoisite…"

We rephrased this sentence accordingly.

13. p.5, line 25: Omit "In contrast" at beginning of sentence

We agree and omitted "in contrast".

14. p.5, line 27: "affected" instead of "influenced"

We rephrased this sentence accordingly.

15. p.6, line 5: better: "…are irregular and rather…"

We rephrased this sentence accordingly.

16. p.6, lines 7-8: I think that there is some indication for host control for the upper left hand quadrant (compare Fig. 4d with 4f). Many of the new grains have an orientation which is vaguely similar to the clast, whereas this is clearly not the case of the other pole figures (4e, g).

Please note that we carefully checked single grain measurements and originally displayed scattered pole figures, but now decided to display density plots, following the suggestions of

referee 2. Density plots have been recalculated from odf after segmentation with space group 121. Texture index and pfj are given. All observations can be summarized as follows:

Chapter 4.1. "EBSD measurements of albite in strain shadows were analysed comparing single grain orientations with that of the host, comparing pole figures of scattered measurements as well as density plots recalculated from ODF (Fig. 4d-g). The EBSD data reveal no obvious orientation relationship between new grains within aggregates or a specific relationship between new grains and porphyroclasts, although some new grain orientations might correlate with that of the clast (compare to Fig. 4 f)."

Chapter 5.4. "That few grain orientations in strain shadows are correlating with that of the host crystal is interpreted to be due to the presence of some fragments of the host crystal (Fig. 4d)."

17. p.6, line 18: The term "sawtooth-shaped" is not very good. Sawtooth usually implies some asymmetry in the teeth shape, like "monoclinic" shapes. Perhaps it is better to use "cuspate-lobate" or just "lobate" as a descriptive term for these microstructures.

We adopted this term from Norberg et al. (2011). However, we agree that the term might be problematic, especially as there is no host-control on the dissolution and reprecipitation, which could lead to asymmetric "teeth".The term "lobate" might rather associate to roundish / smoothly curved boundaries, which is not the case here. Therefore, we now use the suggested term "cuspate".

18. p.6, line 19: "into" instead of "through" K-feldspar.

We rephrased this sentence accordingly.

19. p.6, line 19: "lobate" instead of "curved" grain boundaries

We used "lobate" accordingly.

20. p.6, line 24: What do you mean by this sentence? That the cracks terminate at the albite grains or that the albite grains are separated from the host clast? Please explain this better.

"Healed microcracks terminate at new albite grains, which therefore formed after fracturing (arrows in Fig. 5c, d). "

21. p.6, line 28: "aggregate" instead of "aggregates"

We corrected this mistake.

22. p.7, line 3-4: better: "…that they represent healed cracks … misorientation rather than subgrains (Fig. 8a)."

We rephrased this sentence accordingly.

23. p.7, line7: "… (Fig. 8e), particularly for correlated grain boundaries."

We added this specification.

24. p.7, line 17: space after "compositional" and "which" instead of "whis"

We corrected these typos.

25. p.7, line 19: omit "which is"

We omitted "which is".

26. p.7, line 24: "elongated" instead of "lens shaped" (lens is a 3-D term)

We rephrased the sentence accordingly.

27. p.8, line 23: "of" instead of "on"

We corrected this.

28. p.8, lines 22-23: The apatite inclusions are interesting. It is difficult to see the apatite inclusions in the K-spar in the images of Fig. 6, but they seem to be there in some cases. Is it possible that the apatite inclusions are also present in the K-spar and can be used to mark the former clast outline of the K-spar grains?

Indeed, the apatite inclusions can be traced into the K-feldspar. This indicates that not only albite replaced K-feldspar, but there was also precipitation of K-feldspar. We will add this observation in the revised manuscript. Whether the apatite inclusionscan be used to outline the original shape of the K-feldspar is, however, from our point of view too vague.

"The apatite inclusions are in some places also present in the K-feldspar (Fig. 6b, arrows). "

29. p.8, line 24: o.k, the replacement is not directly related to strain, but the stresses will be highest at the grain boundary, so that in a deforming aggregate, the K-spar will be replaced at the highest stress sites.

We agree.

Last paragraph chapter 5.1. "The K-feldspar replacement is independent on the orientation of the boundary to the foliation and stretching lineation and is therefore interpreted to be not directly related to the strain field during deformation, not excluding some influence of higher strain along the boundary compared to within the crystal."

In addition, it is, generally speaking, the higher free energy state of K-spar than albite. Of course, the higher free energy state will result in a higher solubility, but to express it as solubility is a bit unusual as the solubility depends, among other factors, on the fluid composition, which is unknown here.

With the term solubility difference, we want to stress not only the driving force for dissolution of the K-fsp, but also the formation of albite. The higher free energy state depends on many unknown factors as well, see point 1.

30. p.8, lines 29-31. The fact that there are albite grains at the boundary of the K-spar clasts (clear replacement structures, Fig. 5b) and that there are K-spar clasts inside the fractures (Fig. 5d), it is obvious that K-spar is replaced by albite. It may be possible that, in addition to the replacement, some albite might also precipitate from a fluid, but it is not necessarily "more likely" (as expressed in the text) than the replacement, for which there is clear evidence.

We agree and deleted "more likely".

31. p.9, lines 2-3: The bending may well be results of microcracking, as outlined in Tullis&Yund 1987. So, it is not necessarily the result of plasticity.

In bent albite grains we did not find evidence of microcracks at light-optical scale and SEM-scales, yet some influence of microcracking can certainly not be excluded. However, to explain the observation of a continuously bent crystal solely by brittle deformation would be from our point of view too speculative. See also comments to points 34 and referee #2. We will discuss this when revising the manuscript more comprehensively.

"Bent twins are corresponding to an undulous extinction indicating a continuous internal misorientation, which is usually taken to result from the presence of geometrically necessary dislocations (e.g., Nicolas and Poirier, 1976; Wheeler et al., 2009), though some microcracking might also be involved, as pointed out by Tullis and Yund (1987). For albite this continuous internal misorientation is not associated to distributed healed microfractures, as observed for K-feldspar (compare Figs. 5 and 7), which indicates the relative higher importance of dislocation glide for the deformation of albite compared to K-feldspar."

32. p.9, line 9: Dislocation glide combined with recrystallization (e.g. strain induced grain boundary migration) constitutes, by definition, dislocation creep. Phrased in the way it is written here, the statement is neither correct nor what you want to say. It should be made clear (also in the following discussion section) that the two events (e.g. cracking or glide of dislocations and the replacement/re- or neocrystallization) are different events or episodic processes, otherwise the combined processes would constitute dislocation creep.

We fully agree, we mean a sequence of events, i.e. fracturing and dislocation glide followed by growth (e.g. strain-induced grain boundary migration or growth rims resulting in a SPO). Indeed, this is one of our main point. Please see general comment and point 35.

"Strain-induced grain boundary migration following dislocation glide and microfracturing is consistent with an orientation scatter around the orientation of the host porphyroclast (Fig. 8d, f)."

33. p.9, lines 10-12: I agree with this statement, and you are showing in Fig 11 and 13 that there are chemical differences in grains and overgrowth rims. So, chemical effects will be part of the driving potential.

We agree.

34. p.9, 12-14: As pointed out above, the bending may be the result of microcracking. In addition, the discrete boundaries of misorientation are visible in Fig. 7a (lower arrow marks a

discrete misorientation boundary), and in Fig. 8a (many sharp boundaries between dark and light blue). Furthermore, the fragmentation of the albite clast is clearly visible in the Figs. 7 and 8). The brittle deformation induces defects, too. So, certainly low temperature glide processes may occur, but the evidence shown documents primarily cracking processes.

We agree that cracking is clearly documented by the albite microstructures, as described in chapter 4.3 and 5.2. Albite is showing characteristically a mixture of new grains (strain-free) and fragments (twinned, bent, see Fig. 7 and 8) along boundaries parallel to the foliation. Microcracking can produce dislocations but also dislocation glide can cause micro fracturing. Pile up of dislocations during dislocation glide with ineffective dislocation climb (and thus ineffective recovery) causes strain hardening finally leading to brittle fracturing. The relative role of microcracking versus dislocation glide is clearly difficult to assess from our "post-mortem" approach. Yet, qualitatively, bent and twinned grains without any evidence of microcracks on the light-optical and SEM-scales (as observed here for plagioclase) would indicate that dislocation glide plays a more important role than indicated by healed and sealed intragranular microcracks at high angle to the stretching lineation visible on both light-optical and SEM scales (as observed here for K-feldspar, Fig. 5).

We stressed this point in our discussion throughout the manuscript and especially in the discussion (Chapters 5.2 and 5.3), see point 31.

35. p.9, line 28-30: Strain induced grain boundary migration is a recovery or recrystallization mechanism and thus would be part of dislocation creep. Again, as pointed out above, one has to stress the fact that the processes do not occur simultaneously or are not coupled, because dislocation creep is excluded here (for good reasons).

We fully agree and will sharpen and stress our arguments for this sequence of microfracturing and associated dislocation glide followed by grain boundary migration. Please see general comment and point 32.

new version:

"We suggest that albite porphyroclasts deform in the regime of low-temperature plasticity, where dislocation climb is ineffective and where dislocation glide leads to strain hardening and microfracturing. Additionally, dislocations can be induced by microfracturing (Tullis and Yund, 1987). Subsequently, grains grow by strain-induced grain boundary migration, where crystalline volume with higher strain energy is dissolved and strain-free crystalline volumes precipitated, as was also found by Tullis and Yund (1987)."

36. p.9, line 32: The "micro-crush zones" point to an important term in this context: "semibrittle" deformation. I think that this term is perfectly applicable and includes the cracking and replacement/recrystallization aspects.

We agree.

37. p.10, line 5: omit "in contrast" – this is the start of a new chapter.

We omitted "in contrast".

38. p.10, lines 16-18: Myrmekitization typically does not occur below 550C, because an intermediate plagioclase composition is required for that.

We agree.

39. p.10, line21-23: Why only precipitation and not partly replacement? The albite replacing Kspar forms randomly oriented grains (Fig. 5).

We agree that replacement might occur also in strain shadows. Yet, the (micro-)fabrics indicate shortening perpendicular to the foliation and dilation/extension parallel to the stretching lineation of the finite strain ellipsoid. The polyphase aggregates in strain shadows are taken to indicate precipitation of material that has been dissolved from boundaries parallel to the foliation. Yet, replacement probably occurs as well, which is now mentioned in addition in the revised manuscript.

"Additionally, some replacement might also occur in strain shadows."

40. p.10, lines 28-31: Do you refer to phase mixing by grain boundary sliding?This mechanism is not very effective in producing mixing, and nucleation is far more efficient for that. As you have precipitation (including nucleation?), the mixing in the polyphase material may well be produced by this process.

We fully agree, as stated in the text: "In the mylonitic pegmatites reported here, however, no indication of active "phase mixing" is observed and we attribute the occurrence of a polyphase matrix to precipitation." Precipitation includes nucleation, i.e. not only replacement. We refer to Fliervoet (1995), who describes mechanical phase-mixing, though this author does not present a clear explanation of the process. Yet, we argue that we here do not see evidence of any active phase-mixing.

We state this more clearly in Chapter 5.5, second paragraph of the revised manuscript.

The question is: why is the monophase albite aggregate a single phase material?

The next sentence: "Also, the highest strain in the mylonitic pegmatites is associated not with a polyphase matrix but with the monophase quartz and feldspar layers." is used as connecting passage to discuss the monophase albite aggregates in the following Chapter 5.5.

42. p.11, lines 28: It seems necessary to include at least a short discussion about what may cause the difference between type A and B microstructures. As everything is documented carefully and in detail, the reader is left without a conclusion concerning these differences.

Chapter 5.5, last two paragraphs "Quartz layers of coarse recrystallized grains systematically correlate with albite layers of small isometric grains in the type A matrix microstructure (sect. 4.4; Figs. 9a, b; 10; 11). In contrast, narrow quartz layers with fine-grained quartz aggregates and marked CPO are correlated with elongate coarser albite in the type B matrix microstructure (sect. 4.4; Figs. 9c, d; 12; 13).

The elongate shape of albite and zones of high porosity at boundaries at high angle to the stretching lineation in the type B matrix microstructure indicates growth by precipitation (Fig. 13e, f). The microstructure correlates with the overall strain of the mylonitic matrix (Fig. 14). "

43. p.12, lines1-2: What is the difference between "strain-induced replacement of albite with granular flow" and "dissolution precipitation creep"? The old albite (or K-spar) has to be dissolved in some way, and the replacement corresponds to a precipitation. So, given the fact that chemical changes are involved, it still is a type of dissolution precipitation creep process.

The differencecan be expressed as follows:

 "Dissolution precipitation creep" refers to dissolution at boundaries parallel to the foliation and precipitation with nucleation at areas at high angle to the stretching lineation, which usually results in polyphase aggregates in strain shadows.

"Strain-induced replacement of albite" refers to fracturing and dislocation glide of porphyroclasts along boundaries parallel to the foliation followed by growth by strain-induced grain boundary and involving precipitation to form grains with high aspect ratio with the long axes in the foliation. The results are monophase aggregates.

Because of the characteristically different microstructures and the characteristic sequence for"Strain-induced replacement of albite" (see points 32, 35, 36) with fracturing and dislocation glide followed by growth involving precipitation (including chemical driving forces in addition to strain) we feel that this difference is important.

We strengthened this difference when revising the manuscript, as this is one of our main points, see especially the new discussion in Chapter 5.6.

Response to referee commentsRC2 Solid Earth se-2018-81

The authors gratefully acknowledge the critical and constructive comments by Dr.Rüdiger Kilian. In the following, we respond to each of the points raised. The *comments by the referee are given in cursive characters*, our response in blue, specific changes in the revised manuscript in red. You will find an annotated pdf-file of our revised manuscript below, in which all changes are correlated to the reviewer's comments.

1) "Rheologically dominant processes" and strain The author set the scope of the manuscript to identify the rheologically governing processes (e.g. p1,l3; p3,l13, p11,l29ff). It is noted that monophase layers define the "mylonitic microstructure and clearly correlate with strain". However, it remains unclear 1) how strain is determined (overall in the manuscript when reference is taken to "high strain" or "low strain") and b) which is the rheologically governing process. Dissolution-precipitation creep is a deformation mechanism, granular flow can be a mechanism or a process, quartz layers deforming by dislocation creep are another ingredient to bulk rheology of a rock. Which one out of all of these mechanisms in now dominant, is from my point of view still very open - and for a given mechanism, which process dominates the rheology is also not accessed. For example, does "dissolution-precipitation creep with granular flow" mean- so any interpretation based on those relations are rather speculations or somewhat vague?

Concerning the first comment on strain, please see answer to point 7, as the relative strain is indicated by the width of the alternating quartz-albite layers referring to the "end-member matrix microstructures.

Concerning "rheologically dominant processes", we agree that with our "post-mortem" approach it is difficult to quantitatively judge the role of several fundamental deformation mechanisms and associated processes. The goal of this study is to correlate specific microstructures to different processes and to evaluate how the microstructure evolved. From our findings, we discuss some aspects on the rheological behaviour through the deformation history, which we feel are a relevant outcome of our study.

This is now more carefully phrased throughout the manuscript (please see annotated pdf-file) and especially discussed in Chapter 5.6., now headed: "Implications for rock rheology and deformation history".

2) Similarly, (e.g. p11, l23): "growth parallel to the stretching lineation" , the stretching lineation is finite strain, why would a grain grow towards this direction? Similarly "sites of shortening" appears multiple times in the text should refer rather to to e.g. contractional quadrant (in relation to prophyroclasts), surfaces at a high angle with respect to the inferred principal shortening direction or similar, but I'd argue a site of shortening is something like a point, and hence it does not make sense to refer to shortening of a point.

We used "site" rather in the sense of a volume and were not referring to a point. We usually refered to a crystalline volume close to boundaries of porphyroclasts parallel to the foliation (perpendicular to *z*).

We now refer to boundaries parallel to the foliation, boundaries perpendicular to the stretching lineation and/or strain shadows throughout the revised manuscript.

3) Dislocation glide in albite: Bending of kfs is suggested to be mainly due to microfracturing while bending of albite porphyroclasts should primarily relate to dislocation glide. While microfracturing in Kfs might have been identified in the SEM or thinsection (?both, see Fig. 5), I do not see on which data, the absence of microfracturing in favour of dislocation glide in albite is based on? How was microfracturing in ab excluded?

We did not exclude microfracturing of albite. In chapters 4.3 and 5.2 we describe albite porphyroclasts that show characteristically a mixture of fragments (twinned, bent, see Fig. 7 and 8) and strain-free new grains along boundaries parallel to the foliation, resembling "micro-crush zones" described in Tullis and Yund (1987). Microcracking can produce dislocations but also dislocation glide can cause micro fracturing. Pile up of dislocations during dislocation glide with ineffective dislocation climb (thus ineffective recovery) can cause strain hardening finally leading to brittle fracturing. The relative role of microcracking versus dislocation glide is clearly difficult to assess from natural microstructures. Yet, qualitatively, bent and twinned albite porphyroclasts without any evidence of microcracks on the light-optical and SEM-scales together with the albite replacement in "micro-crush zones" at boundaries parallel to the foliation would indicate that dislocation glide plays a more important role for their formation in comparison to the formation of healed and sealed intragranular microcracks at high angle to the stretching lineation visible on both light-optical and SEM scales (as characteristically observed here for K-feldspar, Fig. 5).

We strengthened this point throughout the manuscript. See also comments to referee #1 (points 31 and 34) and point 38 below.

Chapter 5.2: Strain-induced replacement of albite

"...Bent twins are corresponding to an undulous extinction indicating a continuous internal misorientation, which is usually taken to result from the presence of geometrically necessary dislocations (e.g., Nicolas and Poirier, 1976; Poirier, 1985; Wheeler et al., 2009), though some microcracking might also be involved, as pointed out by Tullis and Yund (1987). For albite this continuous internal misorientation is not associated to distributed healed microfractures, as observed for K-feldspar (compare Figs. 5 and 7), which indicates the relative higher importance of dislocation glide for the deformation of albite compared to K-feldspar."

4) Absence of an orientation relation between ab and kfs (p6,l21): The authors present polefigures for three crystal directions (a partial representation of the full crystal orientation e.g. Fig 6e) to discard an orientation relationship between e.g. kfs and albite. However, pole figures are not the suitable object to explore such relationships. Most easily, orientation relations are explored in misorientation space (for example see Krakow et al, 2017). Additionally, as far as I can tell from Fig. 6e, there is quite a lot of coincidence between kfs and ab directions in the pole figures already, so how comes that such a conclusion is drawn?

We agree that full misorientation space would probably be most telling. For triclinic minerals, this is unfortunately not easy to visualize. In the revised Fig. 5 (which the referee is probably referring to), we present angle and axis distribution separately and also color-code the phase boundaries according to their misorientation angles. Independent on the way to visualize the EBSD data, a systematic crystallographic relationship between the new grains (green) and the original K-feldspar clast (yellow) is not evident.

5) Kfs replacement is independent on specific direction and hence not directly related to strain (p8,l23): How is the rotation of porphyroclasts excluded? I do not see a strong argument here, also no quantitative data to support or reject this claim.

We do not exclude rotation of porphyroclasts, which to some extent appears likely in mylonites. However, we argue that the replacement is not influenced by the orientation of the porphyroclast in the strain field, as the cuspate-phase boundaries to albite occur symmetrically at the boundary of the porphyroclast. If replacement would be significantly influenced by a specific orientation to the strain field, such a symmetric pattern would be difficult to explain by rotation of the porphyroclast with respect to the foliation. Furthermore, the replacements are cut-off by microcracks that occur exclusively at high angle to the stretching lineation (Figs. 5; 6). In addition, the elongate shape of the K-feldspar porphyroclasts with the long axis being parallel to the stretching lineation of the finite strain ellipsoid, excludes major rotation of the porphyroclastindependently to its surrounding after the formation of these microstructures.

6) Interface-coupled dissolution-precipitation: Conceptually, it has been demonstrated in mostly static environments (see: references in (2) p8,l13ff refer to static features mostly without any deformation involved) and one could argue, that it might be unrelated to strain. However, the opposite argument - because it is apparently independent on (the last state of) strain, it should be icdpc is not tested (see comment on rotating prophyroclasts).

The observed cuspate phase boundary of the K-feldspar to albite indicates replacement by dissolution-precipitation processes at the specific phase boundary, i.e. interface-coupled dissolution-precipitation.

7) "end-member matrix microstructures which correlate with strain" (p1, l18; p7, l13): While the microstructural differences are clearly present, I do not understand where the relation to strain could be established. How was strain measured? How could it be said that one is more strained than theother? Also, do those occur only different samples from different locations - as far as it seems in the way presented here - or could both also be found within the same sample?

We only refer to a relative difference in strain. The correlation is, that albite layers with elongated grains and SPO occur in samples, where monophase quartz layers are narrow (a few tens of μm) and several mm long, where the quartz aggregate is fine-grained (several μm in diameter). As opposed to the fine-grained (several μm in diameter) monophase albite layers with isometric grains that occur to coarse-grained (several tens of μm in diameter) quartz layers that have width of hundreds of μm. These microstructures are sample specific. The variations in the width of alternating monophase albite and quartz layers in thin section, correlate with mesoscopic observation of hand specimen and in the field by the width and spacing of the foliation planes defined by elongate mineral assemblages and is interpreted to reflect strain. We rephrased this more specifically throughout the manuscript and in the last paragraph in chapter 4.4. The distribution of the endmember microstructures is now shown in Fig. 1 and listed in an additional supplementary table (see comments to points 9, 17).

8) A few missing explanations in methods and or /figure captions: - how was grain size established - why was frequency distribution and frequency mean chosen over area weighted

mean? We also checked area weighted, which is now changed in all grain area histograms- how was twinning dealt with in ebsd data wrt grain size or other grain related measures -For grain reconstruction a thresholding value of 10° was used. For grain reconstruction, Dauphiné twin boundaries in quartz are neglected. Evaluating albite grain boundaries in full misorientation space (Krakow et al., 2017) revealed that almost all twins correspond to the albite law and some to the pericline law. Also for grain reconstruction of albite, these twins are neglected by merging along twin boundaries. To evaluate also mean grain orientations, requires to use a higher symmetry, which contains the symmetry element responsible for twinning, which is the point group 121 for albite and 622 for quartz. The mean orientation of the "higher symmetry" grain is the modal orientation of the "lower symmetry" grain. Using the higher symmetry yields the same grain reconstruction result as merging along twin boundaries.why are point plots chosen over properly contoured pole figures. In many cases point plots may not be very useful. We will use contoured pole figures in the new figures - Misorientation angle profiles: Misor. angle to origin - please specify what is meant with the various occurrences of "relative misorientation (angle or map)", " internal misorientation (angle)" –we mean the angle to a reference point or to mean orientation, respectively, as will be described in the caption - the authors note that orientation contrasts camouflages subtle compositional differences in the BSE images, - just adding that the latter then should be, what is seen in CL - so why are then EBSD polished section used for BSE analysis to begin with, if this is a known problem? We checked the grey-scale contrast whether it is derived by compositional or orientation contrasts using EDS and EBSD measurements. BSE orientation contrast is present when there is a difference in orientation, irrespective whether Syton- polished or not. - How were apatite needles identified? P signal in EDX? Yes.

We added the information in the methods-chapter in the revised manuscript.

9) Notes on Figures: Fig. 1: Great to see where samples come from, however out of all of these, only 4 appear in the text. Were the other not suitable or were the selected samples the ones that fit the observation?

All samples were carefully analysed and the systematic and characteristic observationsare described. We do not want to present the same characteristic and systematic observations from all analysed samples.

We added a table (see comments to points 7, 17), which gives some more overview on our comprehensive data. Changes in Fig. 1: We colored the sample numbers according to the type of albite-quartz matrix.

10) Fig. 2: Fractures oriented at small angle to shortening direction - where should that be ? (please indicate shear sense); abbreviation Pl not in the image - see also comments above on fracture orientation

We added in the figure caption that the fracture is indicated by the white arrow in Fig. 2 b and also changed Pl (plagioclase) to Ab (albite). We rephrased to fractures oriented at high angle to the stretching lineation.

11) Fig. 3: Unclear what this figure adds to the overall story of the manuscript. Is it needed?

The figure is intended to give the reader some context on theAlpine metamorphic mineral assemblages. We feel that this information is important even though it does not directly relate to the investigation of feldspar deformation.

12) Fig. 4: Pole plots (d,e,g) cannot should be properly contoured. If the message should be, that they are all different, not to distinguish from uniform etc… a proper contouring is needed as pole plots are hard/not to interpret for this purpose. Why are only pole figures plotted for poles to planes and not for directions? Maybe plotting IPDFs for a reasonable reference direction might be even more telling. "relative misorientation map" -> misorientation angle; also relative to what? An arbitrary reference orientation? Grain size histograms: Why are bins chosen to be so narrow that many of them have populations of just one or two grains? Also, please indicate total number. What is the reasoning for the choice of frequency distribution instead if area fraction?

Changes in Fig. 4:

We present contoured plots, calculated from the ODF, with texture index and pole figure strength as measured. We also give contour intervals now. ODFs were calculated for the mean orientation of grains.Relative misorientation in the map is towards mean orientation, we mention this now in the text. We revised the histograms and now show area fractions.

13) Fig. 5: (e) Pole figures are not very suitable to establish/discard any orientation relationship between the two phases. Maybe colorcoding the misorientation angles might be more telling - or better, colorcoding either for the full misorientation or e.g. misorientation axis might be more telling.

See point 4): We agree that full misorientation space would probably be most telling. For triclinic minerals this is unfortunately not easy to visualize, so we chose to use to present angle and axis distribution separately and also color-coded the phase boundaries according to their misorientation angles.

Changes in Fig. 5:
We colored the grain boundaries between replacing albite and the Kfs porphyroclast according to their misorientation angle and exclude the grains in the fracture. Additionally, misorientation axis and angle distributions are shown for these boundaries.

14) Fig. 5/6: Could it be that the albite growing into kfs is larger than the matrix albite?

From our observation, both populations have a similar size distribution. However, we feel that there are too few albite grains replacing K-feldspar to make a meaningful analysis.

15) Fi. 7: "bent and kinked" Where do I see the difference? Indeed, in this image the change in orientation is rather continuous (i.e., "bent"), however, rarely more abrupt changes in orientation occur, which rather resembles "kinking". Yet, because bending is much more common, we will no longer refer to "kinking". (f) What is the bright phase ? Apatite? Some other Ca-phase? It seems that it grows over the clast-new grains boundary (vertical one at the left side).The bright phase is zoisite, which grows in the rare cases of plagioclase with An-contents up to 14 %. This information will be added in the caption. The zoisite grain is actually

fractured at the boundary between clast and new grain. From the positions of other zoisite grains, it is very likely that the zoisite formed before the new grains.

Changes in Fig. 7:
We now mark the zoisite grains.

16) Fig. 8: (a) relative misorientation -> angle ; also relative to what?Sorry this was mistake, it relative to the mean orientation, this information will be added. As noted in the text, I do not see the necessity that the core-rim orientation gradient in the fragmented clast should relate to crystal plasticity. (see comments to point 3 and comments to referee #1, points 31 and 34). (a)-(b) Why is the choice of grains different. Also, if in (a) only the central big grain is displayed, why does it seem that in (b) several grains occupy the same area? This is a misunderstanding, the choice of grains is not different. In (a) not only the central big grain is colorized, but every albite grain within a maximum misorientation of 30°. We did this exactly because the porphyroclast was fragmented into several grains. (Although, there is still one central grain, which we also used for the pole plot in (c). We will clarify this in the revised manuscript.Red lines being low angle boundaries: In (a), they are barely visible, in (b) it looks like they follow direction which could be consistent with the trend of albite twin boundaries - see also the misorientation profile. Also, comparing (a) and (b), again the segmentation seems to be different i.e. in (a) some of the "low angle boundaries" seem to be actually grain boundaries. So maybe something n the segmentation/ handling of twin boundaries went wrong? Please clarify. Sorry, yes, we made a mistake in labelling, we corrected it and now more clearly display the LAGBs (see comment to point 30). The segmentation is now corrected. The general information is not affected by this. (c) what is thecolorcoding of points in the pole plot? The color-coding is the same as in (a) (d) a proper contouring might be nicer. As we only want to show the orientation of the porphyroclast, we do not think contouring would add any information. (d) a proper contouring might be nicer.As we only want to show the orientation of the porphyroclast, we do not think contouring would add any information. (e) Grain size histogram -> see comment on Fig. 4 (g,h) We revised the histograms and now show area fractions. please indicate that this is most likely misorientation angle to origin.We now indicate this.

Changes in Fig. 8:
For (a) and (b) the grain segmentation with space group 121 is now consistent between both figures. The pole figures in (d) where recalculated from odf and texture index and pfj are given now. We now give an area normalized distribution in (e).

17) Fig. 9: Do both matrix types also occur in one and the same sample? Here it's FH5 and CT599 which come from different locations. Any systematics about their occurrences? The microstructure type B is more common than the microstructure type A and there is a slight different distribution from West-East.

The distribution is now shown in Fig. 1 and in an additional table, we state this information now in the revised text (see comments to points 7, 9).

18) Fig. 10: (d) please provide number of grains, what is contoured (1 point per grain or all points) While contouring is much better than the point plots in Fig.9d, it looks like a broader kernel might be more appropriate. (e) Grain size histogram -> see comment on Fig. 4

We provide the number of grains and we recalculated the contouring with a more appropriate (and broader) kernel, determined by the cross-validation approach provided by MTex.

The pole figures in (d) where recalculated from ODF and texture index and pfj are given now. We now give an area normalized distribution in (e).

19) Fig. 11: (c) So orientation contrast camouflages compositional contrast, so what should be learn from the image? That we can see something in the CL (d) what we might have seen in the BSE if the sample wouldn't have had EBSD-quality polishing?

The BSE signal is showing both, orientation and chemical contrast, independent of Syton-polishing (see also comment to point 7). Orientation contrast does not camouflage compositional contrast inside single grains in this case, but leads to an additional contrast between grains. CL images shows internal structures, which do not cause a strong enough contrast in BSE-images.

20) Fig. 12: Where do color artefacts (center lower part and lower left) in (b) come from?

(c) please use a proper kernel for contouring (e) misorientation angle distribution of "albite" Pole figures of pixels or 1 point-per grain? How many data points? It looks like both, ab and kfs is colorcoded in the ipf map: Is that useful? How should one distinguish both there? "maximum mud …": Maxima of pole figures are often relatively meaningless, especially if a relatively arbitrary kernel seems to be chosen or multiple maxima exist. The 2-norm of the pole figure (sometimes called pfJ) or any other measure that suits the symmetry and application might be better, or any of proper measures for orientation distribution functions.

We think the color artefacts come from a high density of unusual twins (not albite/pericline), which are present in these grains. We could not find these twins at any other occasion.

We will present contoured plots, calculated from the ODF, with texture index and pole figure strength as measured. We also will give contour intervals. ODFs were calculated for the mean orientation of grains. The one Kfs grain will not be colored in IPF-colors any more.

Changes in Fig. 12:
We now exclude Kfs from the ipf-coloring in (b). The pole figures in (c) and (d) where recalculated from odf and texture index and pfj are given now. We now give an area normalized distribution in (f).

21) Fig. 13: "Preferred growth parallel to stretching lineation" Why would it grow parallel to the finite stretching direction - unless the pure shear p.d. contribution is very large shouldn't it grow parallel to the extending ISA and eventually rotate? All figures, where a shear sense is available but not provided, should have nice arrows indicating the shear sense.

Please see also comments to points 28, 46.

Changes in Fig. 14: "Growth, granular flow, dislocation creep of quartz -> SPO, alternating quartz-albite layers"

22) General notes on figures: Please make sure the reproduced quality will be better than in the manuscript. I assume that the authors submitted high quality figures - and I am aware of the eagerness of file size reduction at the cost of quality at the side of the Copernicus graphics office/ layout people - so please double check later, that the quality of figures remains very good.

Thank you, we will take care of that.

23) A few more notes: p1, l12: Doesn't kinking and twinnign indicate that glide can't be too effective in accommodating deformation?

Twinning involves glide of dislocations (e.g., Groshong 1988).

24) p1. l21: layers ... parallel to the foliation rather than lineation

We corrected this.

25) p3,l10ff: The last paragraph of the introduction reads like a conclusion, or at least mentions the processes which are later interpreted based on specific microstructures. Is that intentional?

We rephrased this part.

26) p5. l7: Was ebsd da cleaned of orientation noise? That's usually a good idea before doing KAM/ gKAm

Data was cleaned with a half-quadratic filter before gkam.

This is now more comprehensively described in the methods section.

27) p5, l17: sentence

We changed that sentence to "The K-feldspar is Na-poor (<10%) and rarely shows perthitic exsolution." See also our comment to the first referee (point 11.).

28) p5, l30: dilation or extension? (also in other places, please clarify why you think it is dilation and not simply not sites of e.g. lower P)

In this specific sentence, we refer to "strain shadows".

During dissolution-precipitation creep, boundaries at high angle to the extensional direction are "sites"where new material is precipitated for example in veins or strain shadows, causing dilation/extension in this specific direction and represented in the finite strain state by the stretching lineation *x* (e.g., Groshong, 1988; Passchier and Trouw, 2005,Wassmann and Stöckhert, 2013). See also our response to comment 30.

Groshong, H., 1988. Low-temperature deformation mechanisms and their interpretation. Geol. Soc. Am. Bull. 100, 1329–1360.

Passchier, C.W., Trouw, R.A.J., 2005. Micro-Tectonics. Springer, Heidelberg 159–187.

Wassmann, S., Stöckhert, B., 2013. Rheology of the plate interfaced - dissolution precipitation creep in high pressure metamorphic rocks. Tectonophysics 608, 1-29.

29) p6, l33, p7 1ff: Quantifying lattice bending using a misorientation angle wrt origin as a function of distance is not very satisfying since this may only make sense if it can be reasonably assumed that all misorientation is realised around the same axis and rotations remain so low (or at a given symmetry element) that crystal symmetry does not yet matter.

We give the misorientation angle along a distance in addition to the gKam value, as we find this information more intuitively and indeed it refers to the continuous bending of a crystal that is already visible in polarized light micrograph.

30) p7, l2: LAB parallel to shortening direction: anything quantitative on that? We could not detect continuous LABs in this direction with MTEX. Also, where is the shortening direction? First paragraph of section 4.: "The foliation and stretching lineation are characterized by large fragmented magmatic tourmaline and feldspar, here referred to as porphyroclasts and alternating quartz-, albite- and mica-rich layers (Fig. 2a-d). The plane normal to the foliation and the stretching lineation are taken as the principal axes of the finite strain ellipsoid *z* and *x*, respectively, which are indicated in micrographs."

31) p7, l22: What are (monophase) layers composed of aggregates.

Monophase means just one mineral phase, aggregate means different grains (of the same phase, but this is already included in the term "grain").

32) p7, l29: How were traces of planes related to real 3d boundary planes?

We will make clear, that these straight segments can be parallel to traces of (001) and (010) cleavage planes.

 "Straight segments can be parallel to the traces of (001) and (010) cleavage planes traces, representing energetically favoured boundaries (e.g., Tröger, 1982)." (see point 39)

33) p8, l2: i.. not show an internal orientation contrast ...

The term "internal" is added.

34) p9,l11-15 (but also elsewhere): Observations and interpretations of the authors are mixed with references to the literature in a way making it hard to figure what information is claimed by the authors and what comes from literature. These sections can benefit from a more clear separation of citation and authors interpretation.

We revised the text accordingly.

35) p9. l21: influence of water on diffusion e.g. R&D2004: this most likely relates to gbtransport phenomena, at least it was never demonstrated that it is intracrystalline diffusion,

hence it's a bit of a brave jump to speculate on climb enhanced by the presence of fluid - or the absence

This is a misunderstanding, we did not mean to speculate on the enhancement of climb by the presence of fluid. We referred to findings from the literature and transferred a few of these aspects into the introduction (see point below).

36) p9,l15-26: this is a collection of citations in relation to the inability of dislocation climb and the sluggishness of diffusion in the absence of a hydrous fluid. However, this section might be better placed into the introduction.

We agree and placed a few of these aspects into the introduction.

37) p9,l30: "as opposed to solid state grains boundary migration": please explain/clarify; there needs to be transport across the boundary in each case

Our point was to stress the role of dissolution-precipitation as opposed to for example climb-involved subgrain rotation recrystallization (Drury and Urai, 1990; Schenk and Urai, 2005; Stipp and Kunze, 2008).

Subsequently, grains grow by strain-induced grain boundary migration, where crystalline volume with higher strain energy is dissolved and strain-free crystalline volumes precipitated, as suggested by Tullis and Yund (1987).

38) p10. l1ff(and earlier): While all reasonable in very general terms and something one would expect for such a rock, here a few ingredients to the interpretation are somewhat speculative: a) glide and b) strain induced gbm are not demonstrated. While both may be likely, here it remains a speculation since it is not backed by any (semi) quantitative data

Here, we disagree, the indication of dislocation glide is not speculative (see comments to referee #1 (points 31 and 34 and point 3 above). Dislocation glide is demonstrated, e.g., by twinning (which involves glide of dislocations, e.g., Groshong 1988, see point 23) and the continuous bending of the crystal lattice. Even the formation of "micro-crush zones" sensu Tullis and Yund (1987) involves dislocation glide. It would be much more speculative to argue that continuous bending of a crystal is purely brittle, especially without any evidence of fracturing on SEM and polarized-light microscopic scales.We will discuss this in some detail in Chapter 5.2. Strain-induced grain boundary migration is likely by the presence of new grains that are basically strain-free and not represent fragments of the original clasts, we will further strengthen this important point when revising the manuscript. However, also overgrowth of grains by precipitation parallel to the extensional direction during deformation will be important in addition to strain-induced grain-boundary migration.

39) p10. l8: reaction of fracture to crystal directions: a) How was this investigated? and B) is there any data on that?

For K-feldspar, we investigated this by comparing the orientation of microcracks to EBSD data. See, for example Fig. 5. Fractures in K-feldspar are clearly related to the axes of the finite strain ellipsoid and not to the crystallography of the crystal. For fragmentation of plagioclase in the "micro-crush" zones, however, cleavage fractures might indeed play a role.

new version:

Section 4.4. "Straight segments can be parallel to the traces of (001) and (010) cleavage plane, representing energetically favoured boundaries (e.g., Tröger, 1982)."

Section 5.3 "A preferred crystallographic relation of the intragranular fractures was not detected given their orientation at high angle to the stretching lineation independent on crystallographic orientation (Fig. 5), ruling out a major influence of cleavage fractures."

40) p10, l19: Dilation: Please explain, it this true dilation or low P sites or surfaces near orthogonal to extensional directions?

See comment to comment to point 28.

41) p11,l8: albite aggregates instead of albite taking up some deformation

The aggregates formed from strained albite porphyroclasts…

42) p11, l15: grain boundary sliding: while one can see a few straight boundaries in Fig.13, a) why should they indicate gbs b) how frequent are those compared to others ? Anything more convincing on gbs?

We indeed do not have further microstructural evidence on granular flow except of the fine-grained albite layers deflected around porphyroclasts with minor straight boundaries but mostly lobate boundaries (Fig. 13).

"We suggest that after grain size reduction, the fine-grained albite matrix was undergoing a mixture of dissolution-precipitation processes, microcracking and sliding of grains, commonly referred to asgranular flow(e.g., Behrmann and Mainprice, 1987; Stünitz and Fitz Gerald, 1993; Jiang et al., 2000). Sliding might have occurred along straight boundaries weakly inclined to the foliation (Fig. 13b). Microcracking is indicated by the fractures at high angles to the stretching lineation (Fig. 13a, b, e).The weak zoning of grains (Figs. 11 and 13) suggests the involvement of dissolution-precipitation. Granular flow would also cause weakening of adomainal CPO resulting fromthe replacement of albite porphyroclasts (e.g. Jiang et al., 2000; Hildyard et al., 2011)."

43) p11, l19: Hildyard needs year

 (Hildyard et al., 2011).

44) p11, l25: "Microstructure correlates with strain": again, where does strain come from? How does such a "correlation" manifest? Simply elongated vs more equiaxed grains?

Please see comment to point 7).

45) p11, l25: "The higher ..." Sentence

We corrected the sentence.

46) p11. l27: growth parallel to the stretching lineation: While this does not make a lot of sense for non-coaxial p.d. (see comment 2), why preferred growth? Preferred by what? Crystallography? Where should the "dilation" come from? Anything tested on that? What is the CPO of the most elongated grains, or which crystal direction is parallel to the maximum grain elongation direction?

The observation is: The long axes of grains is within the foliation plane. There is no preferred crystallographic orientation of grains with high aspect ratio (see also comments to points 21 and 28). We rephrased the last paragraph of chapter 5.5. accordingly.

47) Entire section 5.6 does not allow me to understand which by now is the process that dominates rheology.

We rewrote the discussion in this chapter and changed the heading to: "Implications for rock rheology and deformation history.", see point 1.

48) p12, l1: "granular flow" (here and elsewhere) please define your understanding of granular flow within the context of a mylonite. Or do you refer to grain boundary sliding in the sense of Rachinger sliding?

Please see comments to point 42).

49) p12, l7: why probably?

We omitted "probably", as this is indeed too speculative.

50) p12. l7: Please enlighten (probably not in the conclusion) why the lobate boundaries between newly grown albite and kfs should be chemical disequilibrium and not due to other driving forces, i.e. gb-width, porosity variations in kfs, defect densities etc.?

We agree that not only chemical disequilibrium but also other factors do play a role for the replacement and discuss this more comprehensively in the section 5.1. However, as albite does replace K-feldspar, the chemical driving force is an important factor.

Last paragraph chapter 5.1. "The cuspate sawtooth-shaped boundaries between new grains of albite and K-feldspar porphyroclasts are interpreted to indicate interface-coupled replacement (Fig. 6), supported by the porosity and apatite inclusions in albite replacing K-feldspar (Fig. 6b, d). The K-feldspar replacement is independent on the orientation of the boundary to the foliation and stretching lineation and is therefore interpreted to be not directly related to the strain field during deformation, not excluding some influence of higher strain along the boundary compared to within the crystal."

51) p12, l19: Why would glide drive gs-reduction in this combined mixture of mechanisms?

As discussed in section 5.2, dislocation glide in association with microfractures in the sense of low-T plasticity is causing a reduction in grain size similar to the "micro-crush" zone in Tullis and Yund, 1987 (see comments to points 3, 38).

52) p12,l20: "observed tendency of slightly enriched Na-content…" Any data on that?

We mention the range of compositions of both the porphyroclast and new grains (p5,18; p6,l29-30). They overlap with a slight tendency for new grains to be more Na-rich.

53) p12,l22: Why subordinate? The balance between chemical driving force vs. e.g. strain energy depends on a lot of variables. For some variables we might have good estimates while for others, we are simply guessing, i.e. dislocation density and elastic energy added by dislocations during deformation etc.

It is true that many variables are not known and we do not try to ignore this problem. Estimates on the influence of chemical driving forces, consider the chemical differences that we observe as too small to play a significant role (e.g., Stünitz, 1998). We discuss this in Chapter 5.1.

1 Here we show the changes made to the figures and present the new captions.

2

3 *Changes in Fig. 1:* We colored the sample numbers according to the type of albite-quartz
4 matrix.

5

6 Fig. 1: Geologic map of the study area (modified after Mancktelow et al., 2001). The sample
7 numbers are colored according to the type of albite-quartz matrix (see text and Table 1)

8

9

10 Fig. 2: Photograph of polished surface (a) and thin section micrograph taken with crossed
11 polarizers (b) of sample CT599. K-feldspar (Kfs), albite (Ab) and tourmaline (Tur)
12 porphyroclasts are embedded in a fine-grained matrix. Elongate fractured tourmaline crystals
13 are oriented with their long axes parallel to the stretching lineation (x). Fractures are commonly
14 oriented at low angle to the shortening direction (z). White arrows point to strain shadows
15 surrounding porphyroclast and prismatic strain shadows between fragments of tourmaline and
16 feldspar. Black arrow points to mylonitic foliation flowing around strain shadow. (c, d)
17 Polarized light micrographs (crossed polarizers, sample FH5b) showing mylonitic foliation
18 defined by quartz layers (Qz) flowing around garnet (Grt) and albite porphyroclasts (Ab), which
19 are partly disintegrated into a fine-grained albite matrix.

20

21

22 *Fig. 3:* BSE images from sample FH27 showing the typical accessory mineral assemblage in
23 the deformed pegmatites: (a) Ca-rich garnet (Grt2) replacing magmatic Fe-rich garnet (Grt1).
24 (b) Epidote and white mica aligned in the foliation with apatite porphyroclasts.

25

26

27 *Changes in Fig. 4:* All pole figures have been recalculated from odf after segmentation with
28 space group 121. Texture index (TI) and pfj are given now. We now show area fractions for
29 grain size analysis. The reference orientation is indicated.

30

31 *Fig. 4:* (a) Asymmetric strain shadow around albite porphyroclast in sample CT599 in thin
32 section micrograph with crossed polarizers. (b) EBSD-phase map of the same area (quartz: blue,
33 albite: green, K-feldspar: red) and (c) EBSD-relative misorientation map (0-10°) of the albite
34 porphyroclast. Polyphase aggregates occur mostly in the upper left and lower right of the clast.
35 In the other quadrants monophase albite dominates. Pole figures show the orientation of albite
36 in the strain shadow in the upper left quadrant (d), lower left quadrant (e), albite porphyroclast
37 (f) and in the upper right quadrant (g). Grain area distribution histograms of albite in polyphase
38 aggregates strain shadow (h) and in monophase albite aggregates (i).

39

40 *Changes in Fig. 5:* We colored the grain boundaries between replacing albite and the Kfs
41 porphyroclast according to their misorientation angle and exclude the grains in the fracture.
42 Additionally, misorientation axis and angle distributions are shown for these boundaries.

43

Fig. 5: K-feldspar deformation microstructures (sample CT599). (a, b) Polarized light micrographs (crossed polarizers) of bent K-feldspar porphyroclast with healed microcracks parallel to the shortening direction and cuspate grain boundaries (white arrows in (b)). (c) Polarized light micrograph (crossed polarizers) showing K-feldspar with fractures filled with albite (black arrow) and cuspate phase boundaries. Healed microcracks are cut-off by newly formed albite (white arrow). Yellow rectangle shows area of EBSD map in (d). (d) EBSD map, where boundaries between replacing albite grains (green) and the K-feldspar-host (yellow) are colored after their misorientation angle. Quartz in the matrix is blue in color. (e) Polefigures of poles to (100), (010) and (001) planes of new albite grains (green) and K-feldspar porphyroclast (black). (f) Misorientation angle and axis distribution for the boundaries colored in (d).

Fig. 6: (a) Photomicrograph of cuspate interface (arrows) between K-feldspar clast and new albite grains (sample CT599). (b) Close-up BSE-image of location indicated by white box in (a). Note the tiny apatite inclusions in the albite (determined by EDS, arrows). (c) BSE-image of cuspate interface between albite replacing K-feldspar in sample FH14. The arrows point to protrusions. (d) Close-up BSE-image of white box in (c) showing the numerous tiny (< 5 μm) apatite inclusions in the replacing albite.

Fig. 7: (a) Polarized light micrograph (crossed polarizers) of bent twins in albite porphyroclast, sample FH5. Fractures occur at high angle to the shortening direction (arrows) (b) BSE image of new albite grains occurring along fractures (arrow). (c) Polarized light micrograph (crossed polarizers), showing fragmented albite porphyroclast partly replaced by new grains and surrounded by quartz layer, sample FH5. (d) Polarized light micrograph (crossed polarizers) showing twinned albite fragments (arrows) surrounded by fine-grained albite matrix, sample FH5. (e) Polarized light micrograph (crossed polarizers) of twinned and fractured albite porphyroclast, sample UP3. Green box indicates area of BSE image in (f), violet box indicates EBSD map shown in Fig 8. (f) BSE image showing new albite grains adjacent to the albite porphyroclast. New grains often have an outer rim of less albitic plagioclase, up to An20 (arrows). The bright phase are zoisite needles.

Fig. 8: (a, b) EBSD-relative misorientation map for albite relative to the mean orientation of the porphyroclast (a) and grain kernel average misorientation (gKAM)-map, showing a lower

87   inferred dislocation density for new grains (b) of the area in the violet box in Fig. 7b. Red lines
88   in are albite and pericline twin boundaries. (c, d) Corresponding pole figures colour coded
89   corresponding to EBSD-relative misorientation map (c) and scatter plot (color-coded
90   corresponding to (a)), where only grains smaller than 100 μm and free of visible twins were
91   used. (e) Grain area distribution for new grains smaller than 100 μm. (f) Misorientation angle
92   distribution for adjacent and random pairs of new albite grains. (g, h) Misorientation profiles
93   (relative to origin) along lines shown in (b).
94
95
96   *Fig. 9:* Polarized light micrographs taken with crossed polarizers showing the two types of
97   quartz-albite matrix microstructure. (a, b) Type A matrix is characterized by coarse quartz
98   layers and albite layers with isometric small grains, sample FH5. (c, d) Type B matrix is
99   characterized by albite layers characterized by coarser and elongate grains parallel to the
100   foliation, and fine grained, dynamically recrystallized quartz layers, samples CT599.
101
102
103   *Changes in Fig. 10:* The pole figures in (d) where recalculated from odf and texture index and
104   pfj are given now. We now give an area normalized distribution in (e).
105
106   *Fig. 10:* EBSD-analysis of type A albite matrix in sample FH5. (a) Photomicrograph of the
107   analysed area. (b) EBSD-map with inverse pole figure colouring (see lower inset). Twin
108   boundaries in the porphyroclast are shown as red lines. (c) Misorientation angle distribution
109   showing an essentially random distribution of neighbouring or random grain pairs. (d)
110   Contoured pole figure showing orientation distribution of albite matrix grains. (e) Grain area
111   distribution of the measured matrix grains. (f) Rose diagram showing the orientation of the long
112   axis of grains. (g) Pole figure showing the orientation of the albite porphyroclast from (a, b).
113
114
115   *Fig. 11:* Type A matrix, sample FH5. (a, b) BSE images show albite matrix with irregular grain
116   boundaries, porosity and weak zonation (black arrows). In (b), the zonation of the grain in the
117   upper right is truncated, possibly by growth of the grain below (green arrow). (c) BSE image
118   with grey shades representing both, orientation and compositional contrast (bright phase is
119   apatite) and (d) corresponding CL image showing zonations, not visible in the BSE image
120   (arrows). Grain boundaries in the CL image are also associated to darker grey shades.
121
122
123   *Changes in Fig. 12:* We now exclude Kfs from the ipf-coloring in (b). The pole figures in (c)
124   and (d) where recalculated from odf and texture index and pfj are given now. We now give an
125   area normalized distribution in (f).
126
127   *Fig. 12:* (a) Photomicrograph of the type B matrix with coarse monophase albite and fine-
128   grained quartz layers in sample CT599. Quartz and albite layers are offset at the shear band
129   marked red. (b) EBSD-map of the area from (a) with an IPF colour code (Z-axis). Only albite

130   is coloured after the IPF-colour-code. (c) Pole figure for albite grains from (b). (d) Pole figure
131   for quartz grains from (b). (e) Misorientation angle distribution showing an essentially random
132   distribution of neighbouring or random grain pairs. (f) Grain area distribution diagram. (g) Rose
133   diagram of the long axis of albite matrix grains from the area measured by EBSD.
134
135
136   *Fig. 13:* BSE images of albite grains in type B matrix. (a) Overview showing elongate albite
137   grains and some relict Kfs grains (light grey). Note grain boundary affected by a crack in the
138   grain below (arrow). (b) Boundaries can be remarkably straight, especially at low angle to the
139   foliation (black arrow). Healed microcracks at low angle to shortening direction are indicated
140   by increased porosity (white arrows). (c) Apatite needles in albite grains. Apatite rich zone is
141   crosscut by grain boundary (arrow). (d) Albite grains showing Ca-enriched zone, representing
142   growth rim (green arrow represents growth direction) with the former grain boundary preserved
143   by the zonation (dashed line). (e) Grain with twins (dashed arrow). Black arrows point to
144   porosity, which is associated with zonation (white arrow), best seen in the CL image (f). The
145   zonation is probably due to changing contents of trace elements, which cannot be resolved in
146   the BSE image.
147
148
149   *Changes in Fig. 14:* We now write "Associated albite overgrowth + dislocation creep of quartz
150   → alternating quartz-albite layers" in the right part of the image and shortened the description
151   on the left..
152
153   *Fig. 14:* Conceptual sketch of the formation of the mylonitic albite matrix. The contribution of
154   replacement of albite porphyroclasts by albite is larger than that of replacement of K-feldspar
155   (see text for discussion).
156

1 **Deformation of feldspar at greenschist facies conditions – the record of**
2 **mylonitic pegmatites from the Pfunderer Mountains, Eastern Alps**
3
4 Felix Hentschel, Claudia A. Trepmann, Emilie Janots
5

6 **Abstract**

7 Deformation microstructures of albitic plagioclase and K-feldspar were investigated in

8 mylonitic pegmatites from the Austroalpine basement south of the western Tauern Window by

9 polarized light microscopy, electron microscopy and electron backscatter diffraction to evaluate

10 ~~the rheologically dominant~~ feldspar deformation mechanisms at greenschist facies conditions.

11 The main mylonitic characteristics are alternating almost monophase quartz and albite layers,

12 surrounding porphyroclasts of deformed feldspar and tourmaline. The dominant deformation

13 microstructures of K-feldspar porphyroclasts are intragranular fractures ~~parallel to the main~~

14 ~~shortening direction indicated by the foliation.~~at high angle to the stretching lineation. The

15 fractures are healed or sealed by polyphase aggregates of albite, K-feldspar, quartz and mica,

16 which also occur along intragranular fractures of tourmaline and strain shadows around other

17 porphyroclasts. ~~Polyphase~~These polyphase aggregates ~~at sites of dilation~~ indicate dissolution-

18 precipitation creep. K-feldspar porphyroclasts are partly replaced by albite characterized by a

19 ~~sawtooth-shaped~~cuspate interface. This replacement is interpreted to ~~be~~take place by interface-

20 coupled dissolution-precipitation driven by a solubility difference between K-feldspar and

21 albite ~~and is not controlled by strain. In contrast, albite~~. Albite porphyroclasts are replaced at

22 ~~sites of shortening~~boundaries parallel to the foliation by fine-grained monophase albite

23 aggregates of small strain-free new grains mixed with deformed fragments. Dislocation glide

24 is indicated by bent~~, kinked~~ and twinned albite. ~~No~~ porphyroclasts with internal misorientation.

25 An indication of effective dislocation climb with dynamic recovery, for example by the

26 presence of subgrains, ~~a crystallographic preferred orientation or sutured grain boundaries was~~

27 ~~observed.~~is systematically missing. We interpret the grain size reduction of albite ~~at sites of~~

Commented [F1]: Point 1, review #2

Commented [F2]: Point 1, review#1

Commented [F3]: Point 3, review#1

28 shortening to be the result of coupled fracturing, dislocation glide and fracturing (low-

29 temperature plasticity). Subsequent growth is by a combination of strain-induced grain

30 boundary migration. and formation of growth rims resulting in an aspect ratio of albite with the

31 long axis within the foliation. This strain-induced replacement by nucleation and growth

32 leads,(associated dislocation glide and microfracturing) and subsequent growth is suggested to

33 result in the observed monophase albite layers, probably together with granular flow, to the

34 monophase albite layers.. The associated quartz layers in contrast, show characteristics of

35 dislocation creep by the presence of subgrains, undulatory extinction and sutured grain

36 boundaries. We identified two endmember matrix microstructures that correlate with strain.

37 Samples with lower strain are characterized by layers of :(i) alternating layers of a few hundreds

38 of µm width, with coarse-grained quartz and layers with isometric, fine-grained feldspar.

39 Higher strained samples are characterized by narrow alternating layers of (in average 15 µm in

40 diameter) and coarse-grained quartz (a few hundreds of µm in diameter), representing lower

41 strain compared to (ii) alternating thin layers of some tens of µm width composed of fine-

42 grained quartz (< 20 µm in diameter) and coarse elongate albite grains elongated parallel to

43 (long axis a few tens of µm) defining the stretching lineationfoliation, respectively. These Our

44 observations indicate that grain size reduction by strain-induced replacement of albite,

45 (associated dislocation glide and microfracturing) followed by growth and granular flow

46 assisted by fracturing and dissolution-precipitation togethersimultaneous with dislocation creep

47 of quartz are rheologically dominantplaying the dominating role in formation of the mylonitic

48 microstructure.

49

1. Introduction

51 Assessment of the rheological behaviour of the continental crust requires an understanding of

52 grain-scale deformation mechanisms of the main rock-forming minerals at not directly

53 accessible depths. In deep parts of seismically active shear zones (10-20 km) the rheological

Commented [F4]: Point 7, review #2

54 behaviour is controlled by the deformation of granitoid rocks, mainly composed of feldspar and

55 quartz, at greenschist facies conditions. A vast number of experimental studies exist to analyse

56 the deformation mechanisms and to derive flow laws for high-temperature creep of feldspar

57 (e.g. Gleason and Tullis, 1993; Kruse and Stünitz, 1999; McLaren and Pryer, 2001; Stünitz et

58 al., 2003; Rybacki and Dresen, 2004) and quartz (e.g., Jaoul et al., 1984; Patterson and Luan,

59 1990; Gleason and Tullis, 1993; Hirth et al., 2001). However, the extrapolation of

60 experimentally deduced flow laws for monomineralic material to the flow behaviour of

61 polymineralic rocks at geologically reasonable conditions is problematic (e.g., Pfiffner and

62 Ramsay, 1982; Tullis and Tullis, 1986; Paterson, 1987; Jordan, 1988). Also, the application of

63 flow laws to model the rheological properties of the continental lithosphere (e.g. Brace and

64 Kohlstedt, 1980; Kohlstedt et al., 1995) is a matter of debate (e.g., Rutter and Brodie, 1991;

65 Burov, 2007; Bürgmann and Dresen, 2008; Burov, 2011). Uncertainties in models for the

66 rheological properties of the continental lithosphere is partly due to a poor knowledge of the

67 deformation mechanisms actually proceeding at depth as well as the interplay between multiple

68 factors influencing rock strength such as stress variations, fluid content, and metamorphic

69 reactions. The comparison of experimental results with microstructural and mineralogical

70 observations of exhumed metamorphic granitoid rocks, which record the grain-scale

71 mechanical and chemical transformations at depths, is therefore indispensable.

72 The extrapolation of experimental flow laws for dislocation creep of quartz to natural conditions

73 is found to agree well to natural observations (e.g., Stöckhert et al., 1999, Hirth et al., 2001,

74 Stipp et al., 2002). However, there are large discrepancies in experimental and natural

75 observations on the most abundant mineral of the continental crust, feldspar. Deformation

76 experiments suggest that dislocation creep of feldspar in high strain shear zones is dominant

77 only at high temperatures above about 900°C (e.g., Rybacki and Dresen, 2004). In contrast,

78 ductile deformation with grain-size reduction and formation of new feldspar grains, commonly

79 assumed to imply dislocation creep, is observed already at greenschist facies conditions (Voll,

80   1976; Tullis, 1983; Gapais, 1989; Stünitz, 1993; Prior and Wheeler, 1999; Ishii et al., 2007).

81   This discrepancy is partly due to the unclear and strongly varying contribution of brittle,

82   dissolution-precipitation and crystal-plastic processes (e.g., Tullis and Yund, 1987; Fitz Gerald

83   and Stünitz, 1993; Stünitz and Fitz Gerald, 1993; Tullis et al., 1996; Prior and Wheeler, 1999;

84   Kruse and Stünitz, 2001; Ree et al., 2005; Menegon et al., 2006, 2008; Stünitz et al., 2003;

85   Mehl and Hirth, 2008; Sinha, et al., 2010; Kilian et al., 2011; Brander et al., 2012; Mukai et al.,

86   2014; Eberlei et al., 2014). Such a creep behaviour governed by the interaction of different

87   deformation mechanisms and chemical reactions in the presence of fluids is especially difficult

88   to assess in experimental approaches. This is partly because experiments have to be performed

89   at high temperatures to realize feasible strain rates, which, however, affects phase assemblages

90   and material properties, for example by partial melting. Therefore, activated mechanisms may

91   strongly differ from those at natural strain rates and greenschist facies conditions. Tullis and

92   Yund (1987) found in their deformation experiments at strain rates of 10^{-4} s^{-1} to 10^{-6} s^{-1} effective

93   dislocation climb with subgrain formation and subgrain rotation only effective at temperatures

94   >900°C. They concluded that optically visible subgrains in feldspar from low-grade rocks

95   should not directly be assumed to arise from crystal plasticity but may arise from cataclasis and

96   subsequent healing. Dislocation climb necessary for dynamic recovery and recrystallization

97   requires intracrystalline diffusion. At temperatures <550°C, the NaSi ↔ CaAl interdiffusion

98   rates for plagioclase are very low (Yund, 1986; Korolyuk and Lepezin, 2009). In the presence

99   of water, the diffusion coefficient has been interpreted to be higher (Yund, 1986), which was

100   suggested to account for the weakening observed in experiments where fluid is present (e.g.

101   Rybacki and Dresen, 2004). TEM studies also show that sufficient dislocation climb to produce

102   subgrains iseffective only at temperatures from the middle amphibolite upward (e.g. White,

103   1975; Stünitz et al., 2003). However, whether anThe experiments by Tullis and Yund (1985)

104   show that grain boundaries may migrate into areas of higher dislocation density introduced by

105   microfracturing driven by the reduction in strain energy (Tullis and Yund, 1987) at conditions,

at which recovery is not active. However, whether extrapolation to natural conditions is valid can only be evaluated by a comparison to natural microstructures.

To analyse the deformation behaviour of feldspar at greenschist facies conditions, we use in this study the record of mylonitic pegmatites of the Austroalpine basement south of the western Tauern Window and north of the Periadriatic line (Fig. 1). They show a wide range of feldspar deformation microstructures and are compositionally and mineralogically relatively simple, as they are characterized by a Ca-poor bulk-rock composition (Stöckhert, 1987). We distinguish specific feldspar microstructures that represent the replacement of large deformed feldspar porphyroclasts in mylonitic pegmatites driven by stored strain energy and chemical disequilibrium and which in combination with fracturing, dislocation glide, grain boundary migration and dissolution precipitation creep form specific types of feldspar-quartz matrix microstructures. The aim is to detect specific microstructures that can be related to processes that govern the rheological behaviour of the rocks. The goal of this study is to correlate characteristic microstructures to specific processes responsible for their formation and to discuss the rheological behaviour of the rocks based on our findings.

2. Geological Settingsetting and Samplingsampling

The pegmatites occur within high-grade polymetamorphic upper Austroalpine basement rocks located between the western Tauern window in the north and the Deferegger-Antholz-Valser (DAV) shear zone in the south (Fig. 1, e.g. Hoffmann et al., 1983; Stöckhert, 1987; Stöckhert et al., 1999; Mancktelow et al., 2001; Schmid et al., 2004; Müller et al., 2000). Pegmatite crystallization age is generally assumed to be Permian (262 ± 7 Ma, Borsi et al. 1980) consistent with other pegmatite occurrences in the Austroalpine basement (e.g., Habler et al., 2009; Thöni and Miller, 2009). The pegmatites are characterized by a Ca-poor composition originated from water-rich anatectic melts (Stöckhert, 1987, Schuster &and Stüwe, 2008).

131 The intrusion of the Rensen and Rieserferner tonalites and related magmatic dikes into the

132 Austroalpine basement rocks took place at ca. 30 Ma (Borsi et al., 1978; 1979; Steenken et al.,

133 2000). ~~The DAV shear zone was active at about the same time~~The amount of uplift and erosion

134 since the intrusion of these magmatic bodies is increasing from about 10 km in an eastern area

135 of the Rieserferner to about 15 to 25 km in the Rensen area in the west (Trepmann et al., 2004).

136 The main activity of the DAV shear zone was at about the same time as the magmatic intrusions

137 and is characterized by an oblique strike slip movement with some tens of kilometres of

138 horizontal component (sinistral sense of shear) and a few kilometres of vertical component,

139 where the northern part of the Austroalpine basement is uplifted relative to the southern part

140 (Borsi et al., 1978; Kleinschrodt, 1987; Schulz, 1989; Ratschbacher et al., 1991; Stöckhert et

141 al., 1999; Mancktelow et al., 2001). It is accompanied by smaller sinistral shear zones to the

142 north, some of which were already active in the Eocene (Mancktelow et al., 2001). The DAV

143 shear zone is viewed as part of the Southern limit of Alpine Metamorphism (SAM) as defined

144 by Hoinkes et al. (1999). To the north of the DAV shear zone, tertiary ages for several mineral

145 systems are widespread (Mancktelow et al., 2001; Schulz et al., 2008) and the metamorphic

146 conditions are constrained to 450±50 °C and pressures of about 0.7 GPa by phase relations in

147 the metapelitic Austroalpine basement rocks (Stöckhert 1982; 1987; Schulz et al., 2008; unpubl.

148 data). ~~Additionally, the northern part shows an increase in exhumation depth towards the west~~

149 ~~(Trepmann et al., 2004).~~ South to the DAV shear zone, the Austroalpine basement rocks have

150 been solely affected by minor metamorphism associated with brittle deformation, in accord

151 with no resetting of the Rb/Sr biotite Permian ages of 288-299 Ma (Borsi et al., 1978; Stöckhert,

152 1982; Kleinschrodt, 1987; Schulz, 1994).

153 The association of the deformation microstructures recorded by the pegmatites ~~with the~~withthe

154 Alpine history is discussed controversially (e.g., Mancktelow et al., 2001; Schulz et al., 2008).

155 Stöckhert (1982, 1984, 1987) proposed that the annealed quartz and feldspar microstructures in

156 the mylonitic pegmatites correlate to an early Alpine deformation stage at metamorphic

temperatures of 450±50 °C, pressures of about 0.7 GPa and at about 100 Ma (white mica K-Ar data, Stöckhert, 1984). This age corresponds to the Eoalpine (Cretaceous) tectonometamorphic event recorded from other units of the Eastern Austroalpine basement (e.g. Thöni and Miller, 1996; Habler et al., 2009). A later (Oligocene) deformation stage at 300 to 350°C was proposed by heterogeneous high-stress quartz microstructures in quartz-rich lithologies of Austroalpine basement rocks related to the movement along the DAV shear zone (Stöckhert, 1982, 1984; Kleinschrodt, 1987; Stöckhert et al., 1999). Mancktelow et al. (2001), however, argued, based on microstructural and kinematic studies, that the deformation microstructure of feldspar could also be Paleogene in age and they find no clear distinction between separate low- and high-T events.

We sampled about 100 pegmatites in three field campaigns in 2015 and 2016. Their appearance varies mostly between m- to cm-sized veins or lenses, and occasionally km-sized bodies occur (Stöckhert, 1987, Hofmann et al., 1983). In a few cases a ~~mineralogical~~ mineral zoning is present. ~~Pegmatites~~Deformed pegmatites, in veins or layers, have a foliation, which is parallel to that of the host gneisses. The largest pegmatite bodies appear macroscopically undeformed. We selected pegmatites with a pronounced foliation and stretching lineation (Fig. 2a; Appendix 1, Table 1). There is no apparent systematic variation in strain with distance to the DAV shear zone, yet the distribution of different matrix microstructures, as described and discussed in sections 4.4. and 5.5., is different from west to east (Fig. 1).

3. Methods

Samples were cut perpendicular to the foliation and parallel to the stretching lineation. Thin sections of ~30 µm thickness were first polished mechanically and then chemo-mechanically in a colloidal silica-solution. For scanning electron microscopy (SEM) thin sections were coated with a thin layer (~5 nm) of carbon. Electron microscopic investigations were performed on a Hitachi SU5000 with a field emission gun. Semi-quantitative chemical measurements by

energy dispersive spectroscopy (EDS, AzTec, Oxford instruments) were acquired using an

accelerating voltage of 20 kV and a working distance of 10 mm. Cathodoluminescence (CL)

imaging using a Gatan MiniCL detector was performed at 5 kV and 10 mm working distance.

Crystallographic orientations were analysed using a HKL NordlysNano high-sensitivity

Electron Backscatter Diffraction (EBSD) detector (Oxford Instruments). The EBSD signals

were acquired using the AzTec analysis software (Oxford instruments). We used a sample

holder pre-tilted at 70° with respect to the electron beam, an accelerating voltage of 20 kV and

a working distance of 20 - 25 mm. The step size for automatic mapping was in the range of 1-

2 µm, dependent of the required resolution, grain size and size of the area measured.

Pole figures were calculated using HKL Channel 5 software (Oxford instruments) and the

MTEX software (Bachmann et al., 2010) from the raw EBSD output. The latter software was

used to colour EBSD maps and for misorientation analysis. For grain reconstruction a

thresholding value of 10° was used. EBSD data were analysed with the MTEX toolbox for

Matlab, developed by Ralf Hielscher (https://mtex-toolbox.github.io/; e.g. Bachmann et al.,

2010). Small non-indexed pixels were filled during data smoothing by a half-quadratic filter

(Bergmann et al., 2015). For grain reconstruction a thresholding value of 10° was used. For

grain reconstruction, Dauphiné twin boundaries in quartz are neglected by merging grains along

boundaries characterized by a misorientation angle of 60° and a [0001] rotation axis. Evaluating

albite grain boundaries in full misorientation space (Krakow et al., 2017) revealed that almost

all twins correspond to the albite law and some to the pericline law. For grain reconstruction of

albite, grains were merged along the corresponding twin boundaries. Evaluating mean grain

orientations neglecting the twin orientations requires the use of a higher symmetry, which

contains the symmetry element responsible for twinning, which is the point group 121 for albite

and 622 for quartz. The mean orientation of the "higher symmetry" grain is the modal

orientation of the "lower symmetry" grain. Using the higher symmetry yields the same grain

reconstruction result as merging along twin boundaries. Grain size analysis was by area

normalization excluding border grains. The mean and median of the area distribution are given in histograms. The aspect ratio and the trend of the grain long axis were calculated from an area-equivalent best-fit ellipse. Pole figures were calculated either from the de-noised EBSD-data (scatter plots) or from orientation distribution functions (ODFs). ODFs were calculated from the grain mean orientation or from every pixel. For the calculation a "de la Vallée-Poussin" kernel was used (https://mtex-toolbox.github.io/; e.g. Bachmann et al., 2010). Kernel width was estimated with the Kullback–Leibler crossvalidation function of MTEX (https://mtex-toolbox.github.io/; e.g. Bachmann et al., 2010). Pole figure densities (pfJ; L2-norm of the pole figures) and texture index (TI, L2-norm of the ODF) are used to characterize texture strength (Mainprice et al., 2015).

For qualitative comparison, we choose to display poles to the (100), (010) and (001) planes in upper hemisphere pole figures for albite. The internal misorientation within grains is dependent on the density of geometrically necessary dislocations and thus is commonly used as a measure of the crystal-plastic strain (e.g. Nicolas and Poirier, 1976; Poirier, 1985; Wheeler et al., 2009). To compare the intragranular misorientation between grains, we used the grain kernel average misorientation (gKAM) (Kilian, 2017), which can be computed in MTEX. The kernel average misorientation is the misorientation angle averaged over a certain kernel width for every measured point. We used a kernel size of 24 pixels (3rd order neighbours) and ignored misorientation angles above 8°, because these are not resulting from low- angle grain boundaries or healed cracks and are thus not related to internal misorientation.°. The sum of these misorientation angles divided by the number of measurements in a grain is gKAM.

Compositions of feldspars and other major minerals were measured by a Cameca SX100 electron microprobe, using 15 kV voltage, 10 nA beam current and 1 µm spot size. The ZAF correction scheme provided by Cameca was used.

Commented [F13]: Points 9, review #1; Points 6, 8, review#2

4. Results

The primary magmatic assemblage of the pegmatite comprises quartz, albite-rich plagioclase, K-feldspar and muscovite with accessory tourmaline, garnet, zircon, apatite and monazite. The foliation and stretching lineation are characterized by large fragmented magmatic tourmaline and feldspar, here referred to as porphyroclasts~~, with their fragments separated parallel to the stretching lineation (Fig. 2a)~~ and alternating quartz-, albite- and mica-rich layers ~~deflected around the porphyroclasts~~ (Fig. ~~2b~~2a-d). ~~Feldspar in~~The plane normal to the ~~mylonitic~~ foliation ~~is 90-95 % albite, independent~~and the stretching lineation are taken as the principal axes of the ~~albite/K-feldspar porphyroclast ratio.~~finite strain ellipsoid z and x, respectively, which are indicated in micrographs. The K-feldspar is Na-poor (<10%) and ~~shows only~~ rarely shows perthitic exsolution. Plagioclase porphyroclasts have a narrow compositional range of Ab_{96-100}. In few samples magmatic plagioclase with Ab_{95-86} ~~occurs, then~~ is present and in these grains zoisite inclusions are common. Magmatic garnet is Mn-rich and low in Ca (on average $Alm_{70}Gro_4Sp_{26}$). During metamorphism, garnet with a higher Ca- and lower Fe-component ($Alm_{35}Gro_{45}Sp_{20}$) partly replaced magmatic grains (Fig. 3a). Epidote and Fe-bearing phengitic white-mica (2 wt% FeO) grew in the foliation plane of mylonitic pegmatites (Fig. 3b).~~ ~~The Fe-bearing phengite sometimes directly replaces magmatic white mica. The modal percentage of albite and K-feldspar varies in the different samples: albite comprises about 60-40 % and K-feldspar about 5-30 %. The matrix layers comprise about 95 % albite, independent on the ratio of K-feldspar to albite porphyroclasts, which varies from 8:1 to 1:9. This observation is consistent with whole-rock compositions with a marked variation of Na_2O and K_2O reported by Stöckhert (1987). ~~In contrast all samples~~Samples show homogenously low CaO (<1 wt.%) and FeO, MgO, MnO (< 1 wt.%) contents (Stöckhert,1987). The variations in the whole-rock composition were interpreted to be due to different compositions of the anatectic melt or mineral zoning in the pegmatite body and ~~influenced~~affected by external fluids (Stöckhert,

Commented [F14]: Points 2, 10, 28, 30, 40, 46, review #2

Commented [F15]: Point 11, review#1

Commented [F16]: Point 12, review#1

Commented [F17]: Point 13, review#1

Commented [F18]: Point 14, review#1

259 1987). In the following, we describe the specific feldspar porphyroclast and matrix

260 microstructures.

261

262 **4.1. Strain shadows**

263 In all samples, polyphase aggregates of K-feldspar, albite, quartz and mica occur in ~~areas of~~

264 ~~dilation~~prismatic strain shadows between tourmaline and feldspar fragments and surrounding

265 feldspar porphyroclasts (Fig. 2b, Fig. 4a, b). Asymmetric strain shadows are characterized by

266 different microstructures displayed in Figure 4a-c: polyphase aggregates of albite, K-feldspar

267 and quartz characterize the upper-left and lower-right quadrants, whereas the lower-left and

268 upper right quadrants contain almost monophase albite aggregates that alternate with quartz

269 layers. This asymmetric strain shadow is indicating a sinistral sense of shear, with the polyphase

270 aggregate representing ~~sites of dilation~~extensional quadrants and the monophase aggregate ~~sites~~

271 ~~of compression~~compressional quadrants. The shape of the albite grains in the monophase layers

272 is rather elliptical with a long axis parallel to the layer, whereas the shape of the albite and K-

273 feldspar grains in the polyphase aggregates are irregular ~~but~~and rather isometric. Grain sizes

274 vary with long axes between 2 and 150 µm, the average of grain diameters is at ~~25 µm~~25µm

275 ($1\sigma = 19$ µm) (Fig. 4h, i). The plagioclase composition uniformly ranges between Ab_{97-100}. ~~The~~

276 EBSD measurements of albite in strain shadows were analysed comparing single grain

277 orientations with that of the host, comparing pole figures of scattered measurements as well as

278 density plots recalculated from ODF (Fig. 4d-g). The EBSD data reveal ~~that there are neither~~no

279 obvious orientation ~~relationships~~relationship between ~~the~~new grains within aggregates ~~nor~~or a

280 specific relationship between new grains and porphyroclasts ~~(Fig. 4e-g)~~., although some new

281 grain orientations might correlate with that of the clast (compare to Fig. 4 f). Generally, the

282 internal misorientation angles of the grains in aggregates with a typical diameter of 25-~~30~~

283 ~~µm~~30µm is low with a maximum internal misorientation generally lower than 5°. The relative

284 misorientation within the albite porphyroclast is lower than 10° (Fig. 4 c).

285

4.2. K-feldspar porphyroclasts

Single fractures in K-feldspar porphyroclasts are sealed by aggregates of K-feldspar, albite and quartz, representing prismatic strain shadows (Figs. 2b, 5c, d). Dispersed fluid inclusion trails at ~~low~~high angle to the ~~shortening direction~~stretching lineation are interpreted as healed microcracks (Figs. 5a-c). Areas comprising a high amount of healed microcracks are associated to undulous extinction, consistent with a bending of the crystal (Fig. 5a). This bending can be quantified by a change in misorientation angle of about 20° over a distance of 700 µm. Yet, in K-feldspar porphyroclasts that do not show dispersed healed microcracks, the internal misorientation angle within one grain is generally below 5° (Fig. 5d) over a grain size of several mm. The K-feldspar porphyroclast interface with new albite grains is ~~„saw tooth"-shaped,~~cuspate due to protrusions of small albite grains ~~through~~ into K-Feldspar over a length of a few tens of µm. Albite protrusions often have ~~curved~~ lobate grain ~~boundaries at~~boundaries at contact with K-feldspar porphyroclast (Fig. 6). The occurrence of this ~~sawtooth-shaped~~cuspate boundary is independent on position with respect to the stretching lineation or ~~shortening direction~~foliation (Fig. 5, 6). EBSD analysis reveals that there is no crystallographic relationship between K-feldspar porphyroclast and new albite grains and the misorientation angle to the porphyroclast is generally high (Fig. 5d, e). The new albite grains often contain numerous pores and inclusions of tiny (< 5 µm) apatite needles, at the vicinity of the K-feldspar porphyroclast interface (Fig. 6b, d). ~~Albite grains along~~The apatite inclusions are in some places also present in the ~~sawtooth-shaped boundaries cut off the healed~~K-Feldspar (Fig. 6b, arrows). Healed microcracks terminate at new albite grains, which therefore are interpreted to have formed after fracturing (arrows in Fig. 5c, d).

308

Commented [F21]: Point 17, review#1

Commented [F22]: Point 18, review#1

Commented [F23]: Point 19, review#1

Commented [F24]: Point 28, review #1

Commented [F25]: Point 20, review#1

4.3. Albite porphyroclasts

Albite porphyroclasts are commonly twinned, ~~kinked~~bent and fragmented (Fig. ~~7). Albite twins~~ ~~are often bent (Figs.~~ 7, 8). The deformed fragments are surrounded by a fine-grained albite ~~aggregates~~ aggregate (grain diameters of 27 µm in average) with a very similar composition (Ab_{96-100}) compared to the host albite, yet with a tendency to a somewhat higher albite component (< 1% higher Ab component). An irregular, patchy An-rich seam (up to An_{20}) is commonly observed around new albite grains (Fig. 7f). ~~The new~~New albite grains occur along fractures ~~and kinks~~ of deformed porphyroclasts that are oriented subparallel to the foliation, i.e., ~~at~~along sites of ~~shortening and~~ high strain and along boundaries parallel to the foliation (Fig. 7a-c, e). The new albite grains are typically not twinned, in contrast to fragments of the host (Fig. 7b, d). Larger host fragments have a relative high internal misorientation with angles typically of about 10° along a profile length of 100 µm, ignoring ~~twinning~~twin domains (Fig. 8g, h). Grain kernel average misorientation (gKAM) values (0.4-0.7 °) for new grains are lower than for the porphyroclast or its fragments (0.7-1) (Fig. 8b). Low-angle boundaries are typically observed oriented ~~parallel~~at high angle to the ~~shortening direction~~stretching lineation, indicating that they ~~rather~~ represent healed cracks associated with a slight misorientation ~~and do not indicate~~ rather than indicating subgrains (Fig. 8a). Curved low-angle boundaries bounding subgrains were not observed. The orientation of the new grains scatters around the orientation of the host crystal (Fig. 8c, d). The misorientation angle distribution shows an excess of low and deficit of high misorientation angles for new grains compared to a random distribution (Fig. ~~8e).~~8e particularly for correlated (neighbouring) measurements).

4.4. Monophase albite matrix alternating with quartz layers

In the fine-grained matrix, layers of almost purely albitic plagioclase Ab_{97-100} (i.e., similar or slightly more Ab-rich compared to plagioclase porphyroclasts) alternate with quartz-rich layers

Commented [F26]: Point 15, review #2

Commented [F27]: Point 21, review#1

Commented [F28]: Point 22, review#1

Commented [F29]: Point 23, review#1

334 (Fig. 9; Appendix 1, Table 1). This mylonitic matrix is often deflected by albite porphyroclast

335 and can also be deflected by albite aggregates replacing former porphyroclasts (~~Sect~~sect. 4.3).

336 The microstructure of the layers differs characteristically in their grain size and shape. Based

337 on these two properties, we distinguish two endmembers of quartz-albite matrix microstructure:

338 Type A) The albite grains in the a few hundred µm wide layers are isometric (aspect ratio: 1 –

339 1.3) with grain diameters varying between 10 – 70 µm, in average of about 15 µm (Fig. 9, 10).

340 The grains usually show no twinning and have a low internal misorientation of generally lower

341 than 5°. The grain boundaries are irregular to smoothly curved (Fig. 11). Inclusions of apatite

342 and domains with high porosity are common (Fig. 11). Grains show compositional zoning

343 (arrows in Fig. 11), which is often only apparent in CL images and is therefore probably linked

344 to changes in trace element contents. This zoning might be truncated by the growth of other

345 grains, ~~which is~~ generally in the direction of their long axes (green arrow in Fig. 11b). A weak

346 shape preferred orientation (SPO) parallel to the foliation can be deflected around the largest

347 porphyroclasts (Fig. 10 a, b). The misorientation angle distribution (Fig. 10c) and ~~pole~~

348 ~~figures~~polefigures (Fig. 10d) reveal a random texture. Associated quartz-layers are typically a

349 few hundred µm wide and composed of coarse-grained aggregates (diameter of 100 – 1000 µm,

350 Figs. 2c, d, 9a,-b).- Quartz in layers shows undulatory extinction, subgrains and sutured grain

351 boundaries (Fig. 9a, b).

352 Type B) The albite grains in the layers typically a few tens of µm wide are ~~lens-shaped~~ elongate

353 (aspect ratio: in average 2.3 and up to 9) and show a marked SPO. The average grain diameter

354 is with 30 µm larger than in the type A microstructure (Fig. 9 c, d, Fig. 12). Similar to the type

355 A microstructure, there is no apparent crystallographic preferred orientation (CPO) of albite

356 and grains have a low internal misorientation (Fig. 12b, c). Some K-feldspar can be present as

357 larger clasts (Fig. 12b) or as irregular flakes (Fig. 13a). The grain boundaries are mostly serrated

358 but can vary to smoothly curved and even straight, then they are at low angle to the foliation

359 (Fig. 13a, b). Straight segments can be parallel to the traces of (001) and (010) cleavage

Commented [F30]: Point 24, review#1

Commented [F31]: Point 25, review#1

Commented [F32]: Point 26, review#1

360 ~~planes~~plane, representing energetically favoured boundaries~~.~~ (e.g., Tröger, 1982). The sutures

361 are affected by intragranular cracks, indicated by ~~trail~~trails of pores at ~~low~~high angle to the

362 ~~shortening direction~~stretching lineation (arrows in Fig. 13a, b). Numerous tiny apatite needles

363 occur in zones generally restricted to the centre of the grains but can be cut off by grain

364 boundaries (Fig. 13c) or microcracks. Rarely, grains with twins occur (Fig. 13e). Some grains

365 show Ca-enriched zones and areas with a higher porosity (Fig. 13e, f). The porosities parallel

366 to the short axes of grains, the elongate shape and the zoning indicate that grains grew ~~parallel~~

367 ~~to the stretching lineation. In general, samples that show the type B matrix record an overall~~

368 ~~higher strain compared to samples with type A matrix, as indicated by the fine-grained quartz~~

369 ~~layers with CPO, which are up to several mm long and a few tens of µm wide (Fig.~~ at boundaries

370 perpendicular to the stretching lineation.~~2a, b, 9c, d, 12a, b, d).~~ Generally, new albite grains do

371 not show an orientation contrast observable by BSE imaging, in contrast to twinned remnants

372 of porphyroclasts (Fig. 7).

373 Samples that show the type B matrix microstructure are interpreted to correlate to a higher strain

374 because of the high aspect ratio (up to 9) and narrow spacing of the alternating quartz-albite

375 layers (tens of µm) compared to the type A microstructure with a larger spacing of the layers

376 of a few hundreds of µm and a lower aspect ratio (Fig. 2a, b, 9c, d, 12a, b, d). These microfabrics

377 correlate with the observation from the field, where samples showing a type B microstructure

378 are characterized by a more narrow spacing of the foliation planes, lower abundance and

379 diameter of porphyroclast as well as a more pronounced stretching lineation.

Commented [F33]: Point 7, review#2

380

5. Discussion

382 In the following, we discuss the deformation and replacement mechanisms of feldspar leading

383 to the mylonitic fabric and implications on the Alpine deformation.

5.1. Interface-coupled K-feldspar replacement by albite

The replacement of K-feldspar by albite is a widely observed reaction in deforming granitoids at low temperatures. Different types of replacements of K-feldspar by albite have been discussed, which can be divided into two groups:

1) Neocrystallisation or heterogeneous nucleation during metamorphic reactions and/or precipitation from the pore fluid, produces distinct albite grains without any crystallographic relationship to the replaced K-feldspar. The replacements often appear in strings and patches inside the host grain and may be related to fractures (e.g. Fitz Gerald ~~&~~and Stünitz, 1993; Stünitz, 1998; Menegon et al., 2013).

2) Interface-coupled dissolution of K-feldspar (or plagioclase) and spatially coupled precipitation of albite leads to a strong structural coherence across the reaction interface, i.e. of the primary mineral on the ~~orientation of~~orientationof secondary mineral as found in rocks (Plümper ~~&~~and Putnis, 2009; Putnis, 2009) and experiments (Norberg et al., 2011; Hövelmann et al., 2010). These studies reported that the new ~~albite might~~albitemight be porous and might contain secondary inclusions. Norberg et al. (2011) observed associated microcracking in the K-feldspar adjacent to the reaction front. The dissolution of K-feldspar has been found to be orientation-dependent (Norberg et al., 2011). ~~Sawtooth-shaped~~Cuspate protrusions of albite growing into the host K-feldspar have been found to be characteristic of such interface-coupled replacements (Norberg et al., 2011).

The ~~sawtooth-shaped~~cuspate boundaries between new grains of albite and K-feldspar porphyroclasts are interpreted to indicate interface-coupled replacement (Fig. 6~~). The~~), supported by the porosity and apatite inclusions in albite replacing K-feldspar ~~support also this assumption~~ (Fig. 6b, d). The K-feldspar replacement is independent ~~on the~~from the orientation ~~to~~of the ~~shortening or~~ boundary to the foliation and stretching ~~lineations~~lineation and is therefore interpreted to be not directly related to the strain~~.~~ field during deformation, not

410 excluding some influence of higher strain along the boundary compared to within the crystal.

411 The driving force is interpreted to be the difference in solubility between albite and K-feldspar

412 at the given greenschist-facies metamorphic conditions (Putnis, 2009). Whereas locally albite

413 grew to replace K-feldspar, K must have been transported through the pore fluid, either to form

414 metamorphic phengitic mica in the foliation plane or to precipitate K-feldspar in polyphase

415 strain shadows (see chapter 5.4.).

416 The albite in grains along intragranular fractures within K-feldspar (Fig. 2b, 5d) might represent

417 neocrystallization of albite replacing K-feldspar. As the intragranular fractures perpendicular

418 to the stretching direction (X)lination (x), these sealed fractures might represent sites of dilation,

419 it is more likely that the prismatic strain shadows, i.e. albite may have precipitated from the

420 pore fluid withoutand not necessarily replacing K-feldspar, i.e. these sealed fractures rather

421 represent strain shadows.

422

423 **5.2. Strain-driveninduced replacement of albite**

424 Albite porphyroclasts are mostly deformed at sites of shortening, commonly associated with

425 dislocation glide indicated by bent mechanical twins (Fig. 7a-e). The areas of high strainAlbite

426 porphyroclasts are mostly deformed at boundaries parallel to the foliation, commonly

427 associated with bent mechanical twins (Fig. 7a-e). Bent twins are corresponding to an undulous

428 extinction indicating a continuous internal misorientation, which is usually taken to result from

429 the presence of geometrically necessary dislocations (e.g., Nicolas and Poirier, 1976; Poirier,

430 1985; Wheeler et al., 2009), though some microcracking might also be involved, as pointed out

431 by Tullis and Yund (1987). For albite this continuous internal misorientation is not associated

432 to distributed healed microfractures, as observed for K-feldspar (compare Figs. 5 and 7), which

433 is taken to indicate a relative higher importance of dislocation glide for the deformation of albite

434 compared to K-feldspar. Strained areas (fractures, porphyroclast boundaries) parallel to the

435 foliation are replaced by new, strain free grains that are generally not twinned (Fig. 7b, d, e-f).

The composition of the new albite grains can be the same as that of the replaced porphyroclast, though it can also show slightly higher Na-content, as already reported by Stöckhert (1987). Plagioclase with Ca-richer compositions occurs locally as thin rims at grain boundaries of new grains with no systematic occurrence (Figs. 7f). Because new strain-free albite grains replace twinned porphyroclasts with internal misorientation at ~~sites of shortening~~boundaries parallel to the foliation (Figs. ~~7e, f, 8a, b~~,) and along intragranular microcracks ~~and kink bands~~ parallel to the foliation (Fig. 7a, b), the replacement is interpreted to be driven by the reduction in stored strain energy. Strain-induced grain boundary migration ~~coupled with~~and formation of growth rims following dislocation glide and microfracturing is consistent with an orientation scatter around the orientation of the host porphyroclast (Fig. 8d, f). The similar composition of the new albite compared to the replaced porphyroclasts, with a tendency of a slightly increased Na-content, suggests a contribution of chemical driving forces although strain-induced grain boundary migration is dominating (Stöckhert, 1982; Stünitz, 1998). Whereas dislocation glide is indicated by bent~~, kinked~~ and twinned porphyroclasts and fragments with internal ~~misorientations~~misorientation, we did not observe subgrains in deformed fragments (Fig. 8a-c), even not in strongly bent ~~and kinked~~ porphyroclasts (Fig. 7 a, b, e~~) and no sutured grain boundaries indicating dynamic "bulging recrystallization" (e.g., Drury et al., 1985; Stünitz, 1998~~). This is consistent with the general finding that albite shows only little evidence of dislocation climb with dynamic recovery and recrystallization at T ≤ 550°C (e.g., Tullis, 1983; Fitz Gerald ~~& Stünitz, 1993; Kruse & Stünitz, 2001).~~ and Stünitz, 1993; Kruse and Stünitz, 2001).~~Dislocation climb necessary for dynamic recovery and recrystallization requires intracrystalline diffusion. At the investigated temperatures (<550°C), the NaSi ↔ CaAl interdiffusion rates for plagioclase are very low (Yund, 1986; Korolyuk & Lepezin, 2009). In the presence of water, the diffusion coefficient is several magnitudes higher, which might account for the weakening observed in experiments where fluid is present (e.g. Rybacki & Dresen, 2004). Only few studies report subgrains in albite deformed at greenschist facies~~

conditions, sometimes together with shear bands (Fitz Gerald & Stünitz, 1993; Eberlei et al., 2014). TEM studies also show that sufficient dislocation climb to produce subgrains is effective only at temperatures from the middle amphibolite upward (e.g. White, 1975; Stünitz et al., 2003). The experiments by Tullis & Yund (1985) show that grain boundaries may migrate into areas of higher dislocation density introduced by microfracturing driven by the reduction in strain energy (Tullis & Yund, 1987) at conditions, at which recovery is not active.

We suggest that albite porphyroclasts deform in the regime of low-temperature plasticity, where dislocation climb is ineffective and where dislocation glide leads to strain hardening and microfracturing. Additionally, dislocations can be induced by microfracturing (Tullis and Yund, 1987). Subsequently, grains grow by strain-induced grain boundary migration, where crystalline volume with higher strain energy is dissolved and strain-free crystalline volumes precipitated, as opposed to solid state grain boundary migration with effective dislocation climb.suggested by Tullis and Yund (1987). Growth can additionally be by precipitation along areas of lower solubility leading to growth rims with a shape-preferred orientation with long axes in the foliation plane. Strain-induced grain boundary migration might be enhanced by chemical disequilibrium (Stöckhert, 1982; Stünitz, 1998). ThisOur interpretation of strain-induced replacement is similar to the "micro-crush zones" described by Tullis &and Yund (1992) associated with undulous extinction, shear bands and grain size reduction that are usually associated to crystal plastic mechanisms (Mclaren &and Pryer, 2001; Stünitz et al., 2003). This process is also similar to the "neocrystallization" in the sense of Fitz Gerald &and Stünitz (1993) and Menegon et al. (2013), which may or may not cause some compositional variations, dependent on the local fluid present. We, however, prefersuggest the term "strain-driveninduced replacement" for the nucleation by low-temperature plasticity (associated dislocation glide and microfracturing) and growth by strain induced grain boundary migrationto stress firstly the importance of dislocation glide (as opposed to the term "micro-crush zones" that stresses brittle mechanisms) and secondly to stress the difference to

Commented [F38]: Point 39, review #1

Commented [F39]: Point 37, review #2

precipitation ~~with nucleation of new phases~~ from the pore fluid ~~at sites of dilation~~ in strain shadows~~.~~ (as opposed to the term "neocrystallization").

5.3. Intragranular fracturing of K-feldspar

~~In contrast,~~ K-feldspar porphyroclasts deformed dominantly by intragranular fracturing with no comparable strain-~~driven~~induced replacement associated with a grain size reduction as observed for albite. ~~Intragranular fractures at low angle to the shortening direction are the dominating deformation microstructures, which did not result in major grain size reduction.~~ A preferred crystallographic relation of the intragranular fractures was not detected, given their orientation at high angle to the stretching lineation independent on crystallographic orientation (Fig. 5), ruling out a major influence of cleavage fractures, ~~although feldspars do show perfect cleavage after (001) and one good cleavage after (010) (e.g., Tröger, 1982).~~ Single fractures are sealed with albite, K-feldspar and quartz representing prismatic strain shadows, or they are healed (Fig. 5). Bending of K-feldspar porphyroclast associated to undulous extinction is restricted to sites of distributed microcracking~~, where some influence of dislocation glide is probable (Fig. 5a).~~ (Fig. 5a).The high amount of healed microcracks at high angle to the stretching lineation indicates that here, microfracturing was dominating over dislocation glide in the bending of the crystal, as opposed to albite porphyroclasts (compare Fig. 5a and Fig. 7 a, e). In contrast to plagioclase, where mechanical twinning is commonly observed, mechanical twinning of K-feldspar is hindered by the Si/Al-ordering ~~and has not been observed~~ (Tullis, 1983).

Reaction weakening of K-feldspar, commonly in association with myrmekites, is known to play a major role during grain size reduction and ductile deformation at many metamorphic conditions (e.g., Simpson and Wintsch, 1989; Tsurumi et al., 2003; Ree et al., 2005; Menegon et al., 2006, 2008, 2013; Abart et al., 2014). In the mylonitic pegmatites described here, myrmekitic replacements are very rare and apart from the ~~sawtooth shaped~~cuspate

514 replacements, K-feldspar porphyroclasts are well preserved. Thus, reaction weakening of K-

515 feldspar is rheologically not relevant for the mylonitic deformation described here.

516

517 **5.4. Precipitation** ~~at sites of dilation~~in strain shadows

518 The occurrence of polyphase aggregates of K-feldspar, albite, mica and quartz ~~located at~~

519 ~~dilatational sites~~in strain shadows between fragments of tourmaline and feldspar

520 porphyroclasts, as well as surrounding porphyroclast (Figs. 2a, b, 4a-c, 5c, d), with random

521 texture and absent systematic crystallographic relationships indicate that these aggregates

522 represent precipitates of a saturated pore fluid during deformation by dissolution-precipitation

523 creep (~~Passchier & Trouw, 2005).~~e.g., Groshong, 1988; Passchier and Trouw, 2005; Wassmann

524 and Stöckhert, 2013). That few grain orientations in the strain shadow correlate with that of the

525 host crystal is interpreted to be due to the presence of fragments of the host crystal (Fig. 4d).

526 The precipitation of K-feldspar, quartz and albite in strain shadows and albite growth rims is

527 restricted to ~~sites of dilation, i.e.~~boundaries at high angle to the stretching lineation (x), i.e.

528 controlled by strain, yet an additional chemical driving force is clearly not ruled out but rather

529 probable. Additionaly, some replacement might also occur in strain shadows. The sites of

530 dissolution are much more difficult to identify, as the material has been removed.

531 A polyphase matrix of K-feldspar, albite quartz and mica in mylonitic granitoids is often

532 attributed to fine-grained reaction products (e.g~~.,~~. Stünitz ~~&~~and Fitz Gerald, 1993; Rosenberg

533 ~~&~~and Stünitz, 2003; Kilian et al., 2011). Other authors, suggest polyphase matrix to develop by

534 mechanical phase mixing in mylonites at highest strain (Fliervoet, 1995). In the mylonitic

535 pegmatites reported here, however, no indication of active "phase mixing" is observed and we

536 attribute the occurrence of a polyphase matrix to precipitation. Also, the ~~highest strain in~~

537 ~~the~~characteristic mylonitic microstructure of the pegmatites is associated not with a polyphase

538 matrix but with the monophase quartz and ~~feldspar~~albite layers.

539

Commented [F42]: Points 2, 10 28, 30, 40, 46, review #2

Commented [F43]: point 16, review #1

5.5. Formation of monophase albite layers

Based on our observations that ~~the~~ albite in layers shows the same characteristics as albite grains replacing albite porphyroclasts (missing subgrains and internal misorientations, apatite inclusions, weak chemical zoning and porosity, and remnants of twinned porphyroclast fragments), we suggest, that the strain-~~driven~~induced replacement of albite is the most important process of grain size reduction to form the monophase albite layers (Fig. 14). Additionally, ~~some~~part of the albite in the mylonitic matrix stems from the replacement of K-feldspar (~~Sects~~sects. 4.2 and 5.1), as suggested by K-feldspar-relicts (Figs. 12b; 13a). Because the matrix layers comprise about 95% albite, independent on the ratio of K-feldspar to albite porphyroclasts, we suggest that albite is taking up a higher amount of strain as compared to K-feldspar. Dislocation creep of albite is ruled out as main process to form the fine-grained almost monophase albite layers, given a missing systematic CPO as well as missing evidence of effective dislocation climb. Also, precipitation from the pore fluid as dominating process can be ruled out, given the monophase composition of the layers, in contrast to polyphase aggregates in ~~dilation sites.~~strain shadows. Cataclasis would suggest a higher amount of twinned and deformed fragments. Instead, only very rarely twinned grains are observed (Fig. 13e).

~~After~~We suggest that after grain size reduction ~~by~~, the ~~strain-driven replacement of~~ fine-grained albite~~,~~ matrix was undergoing a mixture of dissolution-precipitation processes, microcracking and sliding of grains, commonly referred to as granular flow (e.g., Behrmann and Mainprice, 1987; Stünitz and Fitz Gerald, 1993; Jiang et al., 2000~~), i.e. sliding of grains relative to each other probably has played a major role in the fine-grained albite matrix. Straight~~). Sliding might have occurred along straight boundaries weakly inclined to the foliation (Fig. ~~13b) might represent boundaries along which sliding occurred. This and the weak zoning in association with microcracks~~13b). Microcracking is indicated by the fractures at ~~low~~high angles to the ~~shortening direction~~foliation (Fig. 13a, b, e~~) indicate that granular flow was assisted by~~

microcracking and). The weak zoning of grains (Figs. 11 and 13) suggests the involvement of dissolution-precipitation processes. Granular flow would also cause weakening of a domainal CPO resulting from the replacement of albite porphyroclasts (e.g. Jiang and Wheeler,et al., 2000; Hildyard et al., 2011).

Quartz layers of coarse recrystallized grains systematically correlate with albite layers of small isometric grains in the type A matrix microstructure (sect. 4.4; Figs. 9a, b; 10; 11). In contrast, narrow quartz layers with fine-grained quartz aggregates and marked CPO are correlated with elongate coarser albite in the type B matrix microstructure (Sect. 4.4; Figs. 9c, d; 12; 13).

The elongate shape of albite and zones of high porosity at boundaries at high angle to the stretching lineation in the type B matrix microstructure indicates oriented growth parallel to the stretching lineation, i.e. overgrowth at sites of dilation, as indicated by the growth zones associated with porosity parallel to the shortening directionprecipitation, resulting in a shape-preferred orientation (Fig. 13e, f). The microstructure correlates with the overall strain of the mylonitic matrix (Fig. 14). The In samples with higher the overall strain, the coarser and more elongate the albite grains in the layers are coarser and more elongate and the finer-grained quartz aggregates with are finer-grained and have a marked CPO. Therefore, we suggest that the albite grains grew parallel to the stretching lineation, forming a higher aspect ratio by preferred growth.

5.6. Rheologically dominant processes

5.6. Implications for rock rheology and deformation history

The prismatic strain shadows of polyphase material between fragmented tourmaline and feldspar as well as strain shadows surrounding porphyroclastporphyroclasts indicate that dissolution-precipitation creep did play a role in the rheology of the rocks. Yet, other indicators of dissolution-precipitation creep, as for example evidence of dissolved feldspar porphyroclasts

<aside>Commented [F44]: Point 40, review #1, Points 42, 48, review#2</aside>

at sites of shortening, i.e. strain caps, are remarkably low. In contrast, the monophase quartz and albite layers are the main characteristic of the mylonitic microstructure and clearly correlated with strain. Therefore, strain-induced replacement of albite with granular flow and dislocation creep of quartz are interpreted to rheologically dominate over dissolution-precipitation creep. along boundaries parallel to the foliation, i.e. strain caps, are remarkably low. The monophase alternating quartz and albite layers are the main characteristic of the mylonites. The dominating process of grain size reduction of feldspar is interpreted to be the strain-induced replacement of albite with associated dislocation glide and fracturing (Fig. 14). Subsequent growth by strain-induced grain boundary migration and formation of growth rims by precipitation resulted in a SPO (Fig. 14), which took place probably simultaneously together with granular flow and dislocation creep of quartz. As such, for considering the rock's rheology, these different deformation mechanisms and associated processes have to be taken into account, where the relative contributions additionally vary with time. In contrast, dissolution-precipitation creep with dissolution along boundaries parallel to the foliation and precipitation with nucleation of new phases in strain shadows is interpreted to play an only subordinate role for the formation of the mylonitic alternating quartz-albite layers, although precipitation of albite forming elongate grains with SPO in monophase aggregates is important. Furthermore, a major role of dislocation creep of feldspar (i.e., deformation by dislocation glide with simultaneous dynamic recovery) on the formation of the mylonitic microstructure as may be suggested by monophase layers of fine-grained feldspar aggregates, is not supported by any further microstructural observation (e.g., systematic missing of LAGBs) and therefore interpreted to be rheologically not relevant during deformation.

The observation of newly precipitated grains from the pore fluid between tourmaline and K-feldspar fractures at sites of dilation strain shadows as well as the microcracks in K-feldspar that are cut off by the wedge shaped albites replacing K-feldspar (Figs. 2a, b; 3c, d) indicate growth of grains after fracturing and during ongoing deformation. The observation of the deflected

mylonitic foliation around former porphyroclasts, which are now replaced by new grains (Fig. 2c, d; 7c), indicates that the new grains grew after, or more probably, during the formation of the mylonitic layers, but not before. Thus, strain-induced replacement of albite must have played an important role during an early stage of deformation and was ongoing during granular flow. Thus, a specific sequence of different deformation episodes at markedly different metamorphic stages, as had been discussed, is not apparent (Stöckhert, 1987; Mancktelow et al., 2001). The indication of the type A matrix microstructure being dominating in the eastern area and the type B matrix microstructure representing in comparison higher strain in the western area (Fig. 1) might be correlated with higher metamorphic temperature conditions in the western area, as the amount of uplift and erosion since the intrusion of magmatic bodies at 30 Ma is increasing from about 10 km in an eastern area of the Rieserferner to about 15 to 25 km in the Rensen area in the west (Trepmann et al., 2004).

Commented [F45]: General comment and points 42, 43 review #1, points 1, 2 review#2

6. Conclusions

The mylonitic pegmatites record the deformation behaviour of feldspar at greenschist facies conditions. Based on our observations and discussions we draw the following conclusions:

1. K-feldspar porphyroclasts deformed dominantly by fracturing and only subordinate dislocation glide, without major grain size reduction. Healed or sealed intragranular fractures in large porphyroclasts at lowhigh angle to the shortening directionstretching lineation are the dominating deformation microstructures of K-feldspar (Fig. 5).

2. Interface-coupled replacement of K-feldspar by albite is mainly driven by chemical disequilibrium and not by strain, as indicated by the sawtooth shapedcuspate albite-K-feldspar phase boundaries independent on the orientation of the boundary to the foliation or the stretching lineation (Fig. 6).

3. Grain size reduction of albite porphyroclasts is by combined fracturing, and dislocation glide, i.e. low-temperature plasticity. Dislocation glide is indicated by bent and twinned

644 remnant host albites with internal misorientation. Evidence of significant amount of
645 dislocation climb allowing effective dislocation creep with dynamic recovery of
646 feldspar is systematically missing (no subgrains, negligible internal misorientation of
647 new grains; Figs. 10c, d, 12c, e).

648 3.4.Subsequent strain-induced grain boundary migration and formation of growth rims
649 produced aggregates of strain-free albite grains with SPO at sites of
650 shorteningporphyroclast boundaries parallel to the foliation (Figs. 7c-f, 8). The observed
651 tendency of slightly enriched Na-content (decrease of Ca-content) of the new albite
652 grains compared to albite porphyroclasts is in agreement with an additional, though
653 subordinate driving force for grain boundary migration by chemical disequilibrium
654 (Stöckhert, 1982).

655 4.1.Dislocation glide is indicated by bent, kinked and twinned albite with internal
656 misorientation. Evidence of significant amount of dislocation climb allowing effective
657 dislocation creep with recovery of feldspar is systematically missing (no subgrains,
658 negligible internal misorientation of new grains, random texture Figs. 10c, d, 12c, e).

659 5. Granular flow of the new albite grains assisted by fracturing and dissolution-
660 precipitation with overgrowth of albite parallel to the stretching direction in samples of
661 high strain led to the monophase albite ribbons (Figs. 9-13).

662 6.5.Monophase quartz ribbonslayers formed dominantly by dislocation creep (dislocation
663 glide, dynamic recovery and grain boundary migrationrecrystallization) of quartz, as
664 indicated by sutured grain boundaries, CPO, subgrains and undulatory extinction (Figs.
665 2c, 9, 12a, d). Some influence of dissolution-precipitation creep cannot be excluded;
666 though microstructural evidence has not been observed.

667 Although evidence of dissolution-precipitation creep is evident by polyphase strain shadows
668 and sealed fractures of porphyroclasts, the main strain of the mylonitic pegmatites is correlating
669 with the alternating albite and quartz layers. Strain-induced replacement of albite and granular

flow assisted by fracturing and dissolution-precipitation as well as dislocation creep of quartz are the rheologically dominant processes recorded by the pegmatitic mylonites.

    6. Granular flow of the new albite grains with overgrowth of albite forming a SPO together with quartz dislocation creep is interpreted to result in the alternating monophase albite-quartz layers (Figs. 9-13).

For considering the rock's rheology, these different deformation mechanisms and associated processes have to be taken into account, where the relative contributions additionally vary with time.

References

Abart, R., Heuser, D., and Habler, G.: Mechanisms of myrmekite formation: case study from the Weinsberg granite, Moldanubian zone, Upper Austria, Contributions to Mineralogy and Petrology, 168, 1–15, https://doi.org/10.1007/s00410-014-1074-7, 2014.

Behrmann, J. H. and Mainprice, D.: Deformation mechanisms in a high-temperature quartz-feldspar mylonite: evidence for superplastic flow in the lower continental crust, Tectonophysics, 140, 297–305, https://doi.org/10.1016/0040-1951(87)90236-8, 1987.

Borsi, S., Del Moro, A., Sassi, F. P., Zanferrari, A., and Zirpoli, G.: New geopetrologic and radiometric data on the Alpine history of the Austridic continental margin south of the Tauern window (Eastern Alps)., Memorie di Scienze Geologiche, 32, 1–19, 1978.

Borsi, S., Del Moro, A., Sassi, F. P., and Zirpoli, G.: On the age of the Vedrette di Ries (Rieserferner) massif and its geodynamic significance, Geologische Rundschau, 68, 41–60, https://doi.org/10.1007/BF01821121, 1979.

Borsi, S., Del Moro, A., Sassi, F. P., Visona, D., and Zirpoli, G.: On the existence of Hercynian aplites and pegmatites in the lower Aurina valley (Ahrntal, Austrides, Eastern Alps), Neues Jahrbuch für Mineralogie, 11, 501–514, 1980.

Brace, W. and Kohlstedt, D. L.: Limits on lithospheric stress imposed by laboratory experiments, Journal of Geophysical Research, 85, 6248–6252, 1980.

Brander, L., Svahnberg, H., and Piazolo, S.: Brittle-plastic deformation in initially dry rocks at fluid-present conditions: transient behaviour of feldspar at mid-crustal levels, Contributions to Mineralogy and Petrology, 163, 403–425, https://doi.org/10.1007/s00410-011-0677-5, 2011.

Bürgmann, R. and Dresen, G.: Rheology of the Lower Crust and Upper Mantle: Evidence from Rock Mechanics, Geodesy, and Field Observations, Annual Review of Earth and Planetary Sciences, 36, 531–567, https://doi.org/10.1146/annurev.earth.36.031207.124326, 2008.

Burov, E. B.: Plate Rheology and Mechanics, pp. 99 – 151, Elsevier, Amsterdam, https://doi.org/10.1016/B978-044452748-6.00102-4, 2007.

Burov, E. B.: Rheology and strength of the lithosphere, Marine and Petroleum Geology, 28, 1402–1443, https://doi.org/10.1016/j.marpetgeo.2011.05.008, 2011.

Drury, M. R., Humphreys, F. J., and White, S. H.: Large strain deformation studies using polycrystalline magnesium as a rock analogue. Part II: dynamic recrystallisation mechanisms at high temperatures, Physics of the Earth and Planetary Interiors, 40, 208–222, https://doi.org/10.1016/0031-9201(85)90131-1, 1985.

Eberlei, T., Habler, G., Grasemann, B., and Abart, R.: Upper-greenschist facies intragrain deformation of albite in mylonitic meta-pegmatite and the influence of crystallographic anisotropy on microstructure formation, Journal of Structural Geology, 69, 47–58, https://doi.org/10.1016/j.jsg.2014.10.001, 2014.

Fitz Gerald, J. and Stünitz, H.: Deformation of granitoids at low metamorphic grade. I: Reactions and grain size reduction, Tectonophysics, 221, 269–297, https://doi.org/10.1016/0040-1951(93)90163-E, 1993.

Fliervoet, T. F.: Deformation Mechanisms in Fine Grained Quartzo-Feldspathic Mylonites, Ph.D. thesis, Universiteit Utrecht, 1995.

Gapais, D.: Shear structures within deformed granites: mechanical and thermal indicators, Geology, 17, 1144–1147, https://doi.org/10.1130/0091-7613(1989)017<1144:SSWDGM>2.3.CO, 1989.

Gleason, G. C. and Tullis, J.: Improving flow laws and piezometers for quartz and feldspar aggregates, Geophysical Research Letters, 20, 2111–2114, https://doi.org/10.1029/93GL02236, 1993.

Groshong, H., 1988. Low-temperature deformation mechanisms and their interpretation. Geol. Soc. Am. Bull. 100, 1329–1360.

Habler, G., Thöni, M., and Grasemann, B.: Cretaceous metamorphism in the Austroalpine Matsch Unit (Eastern Alps): The interrelation between deformation and chemical equilibration processes, Mineralogy and Petrology, 97, 149–171, https://doi.org/10.1007/s00710-0090094-x, 2009.

Hildyard, R. C., Prior, D. J., Mariani, E., and Faulkner, D. R.: Characterization of microstructures and interpretation of flow mechanisms in naturally deformed, fine-grained anhydrite by means of EBSD analysis, Geological Society, London, Special Publications, 360, 237–255, https://doi.org/10.1144/SP360.14, 2011.

Hirth, G., Teyssier, C., and Dunlap, W. J.: An evaluation of quartzite flow laws based on comparisons between experimentally and naturally deformed rocks, International Journal of Earth Sciences, 90, 77–87, https://doi.org/10.1007/s005310000152, 2001.

Hofmann, K., Kleinschrodt, R., Lippert, R., Mager, D., and Stöckhert, B.: Geologische Karte des Altkristallins südlich des Tauernfensters zwischen Pfunderer Tal und Tauferer Tal (Südtirol), Der Schlern, 57, 572–590, 1983.

Hoinkes, G., Koller, F., Rantitsch, G., Dachs, E., Höck, V., Neubauer, F., and Schuster, R.: Alpine metamorphism of the Eastern Alps, Schweizerische mineralogische und petrographische Mitteilungen, 79, 155–181, 1999.

Hövelmann, J., Putnis, A., Geisler, T., Schmidt, B. C., and Golla-Schindler, U.: The replacement of plagioclase feldspars by albite: Observations from hydrothermal experiments, Contributions to Mineralogy and Petrology, 159, 43–59, https://doi.org/10.1007/s00410-009-04154, 2010.

Ishii, K., Kanagawa, K., Shigematsu, N., and Okudaira, T.: High ductility of K-feldspar and development of granitic banded ultramylonite in the Ryoke metamorphic belt, SW Japan, Journal of Structural Geology, 29, 1083–1098, https://doi.org/10.1016/j.jsg.2007.02.008, 2007.

Jaoul, O. and Tullis, J.: The effect of varying water contents on the creep behaviour of Heavitree Quartzite, Journal of Geophysical Research, 89, 4298–4312, https://doi.org/10.1029/JB089iB06p04298, 1984.

Jiang, Z., Prior, D. J., and Wheeler, J.: Albite crystallographic preferred orientation and grain misorientation distribution in a low-grade mylonite: implications for granular flow, Journal of Structural Geology, 22, 1663–1674, https://doi.org/10.1016/S0191-8141(00)00079-1, 2000.

Jordan, P.: The rheology of polymineralic rocks - an approach, Geologische Rundschau, 77, 285–294, https://doi.org/10.1007/BF01848690, 1988.

Kilian, R. and Heilbronner, R.: Analysis of crystallographic preferred orientations of experimentally deformed Black Hills Quartzite, Solid Earth, 8, 1095–1117, https://doi.org/10.5194/se-8-1095-2017, 2017.

Kilian, R., Heilbronner, R., and Stünitz, H.: Quartz grain size reduction in a granitoid rock and the transition from dislocation to diffusion creep, Journal of Structural Geology, 33, 1265–1284, https://doi.org/10.1016/j.jsg.2011.05.004, 2011.

Kleinschrodt, R.: Quarzkorngefügeanalyse im Altkristallin südlich des westlichen Tauernfensters (Südtirol_Italien), Erlanger geologische Abhandlungen, 114, 1 – 82, 1987.

Kohlstedt, D. L.: Strength of the lithosphere: Constraints imposed by laboratory experiments, Journal of Geophysical Research, 100, 17587– 17602, https://doi.org/10.1029/95JB01460, 1995.

Korolyuk, V. N. and Lepezin, G. G.: The coefficients of heterovalent NaSi-CaAl interdiffusion in plagioclases, Russian Geology and Geophysics, 50, 1146–1152, https://doi.org/10.1016/j.rgg.2009.11.013, 2009.

Krakow, R., Bennett, R. J., Johnstone, D. N., Vukmanovic, Z., Solano-Alvarez, W., Lainé, S. J., Einsle, J. F., Midgley, P. A., Rae, C. M. F., Hielscher, R.: On three-dimensional misorientation spaces, Proceedings of the Royal Society A, 473, https://doi.org/10.1098/rspa.2017.0274, 2017.

Kruse, R. and Stünitz, H.: Dynamic recrystallization processes in plagioclase porphyroclasts, Journal of Structural Geology, 23, 1781 – 1802, https://doi.org/10.1016/S0191-8141(01)00030-X, 2001.

Mainprice, D., Bachmann, F., Hielscher, R., Schaeben, H.: Descriptive tools for the analysis of texture projects with large datasets using MTEX: strength, symmetry and components, Geological Society, London, Special Publications, 409, 251-271, https://doi.org/10.1144/SP409.8, 2014

Mancktelow, N. S., Stöckli, D., Grollimund, B., Müller, W., Fügenschuh, B., Viola, G., Seward, D., and Villa, I. M.: The DAV and Periadriatic fault systems in the Eastern Alps south of the Tauern window, International Journal of Earth Sciences, 90, 593–622, https://doi.org/10.1007/s005310000190, 2001.

Mclaren, A. and Pryer, L. L.: Microstructural investigation of the interaction and interdependence of cataclastic and plastic mechanisms in Feldspar crystals deformed in the semi-brittle field, Tectonophysics, 335, 1–15, https://doi.org/10.1016/S0040-1951(01)00042-7, 2001.

Mehl, L. and Hirth, G.: Plagioclase preferred orientation in layered mylonites: Evaluation of flow laws for the lower crust, Journal of Geophysical Research: Solid Earth, 113, 1–19, https://doi.org/10.1029/2007JB005075, 2008.

Menegon, L., Pennacchioni, G., and Stünitz, H.: Nucleation and growth of myrmekite during ductile shear deformation in metagranites, Journal of Metamorphic Geology, 24, 553–568, https://doi.org/10.1111/j.1525-1314.2006.00654.x, 2006.

Menegon, L., Pennacchioni, G., and Spiess, R.: Dissolution-precipitation creep of K-feldspar in mid-crustal granite mylonites, Journal of StructuralofStructural Geology, 30, 565–579, https://doi.org/10.1016/j.jsg.2008.02.001, 2008.

Menegon, L., Stünitz, H., Nasipuri, P., Heilbronner, R., and Svahnberg, H.: Transition from fracturing to viscous flow in granulite facies perthitic feldspar (Lofoten, Norway), Journal of Structural Geology, 48, 95–112, https://doi.org/10.1016/j.jsg.2012.12.004, 2013.

Mukai, H., Austrheim, H., Putnis, C. V., and Putnis, A.: Textural Evolution of Plagioclase Feldspar across a Shear Zone: Implications for Deformation Mechanism and Rock Strength, Journal of Petrology, 55, 1457–1477, https://doi.org/10.1093/petrology/egu030, 2014.

Müller, W., Mancktelow, N. S., and Meier, M.: Rb-Sr microchrons of synkinematic mica in mylonites: an example from the DAV fault of the Eastern Alps, Earth and Planetary Science Letters, 180, 385–397, https://doi.org/10.1016/S0012-821X(00)00167-9, 2000.

Nicolas, A., Poirier, J.P., 1976. Crystalline Plasticity and Solid State Flow in Metamorphic Rocks. Wiley-Interscience, New York, 444 pp.

Norberg, N., Neusser, G., Wirth, R., and Harlov, D. E.: Microstructural evolution during experimental albitization of K-rich alkali feldspar, Contributions to Mineralogy and Petrology, 162, 531–546, https://doi.org/10.1007/s00410-011-0610-y, 2011.

Passchier, C. W. and Trouw, R. A.: Microtectonics, Springer Berlin Heidelberg, Berlin, Heidelberg, https://doi.org/10.1007/978-3-662-08734-3, 2005.

Paterson, M.: Problems in the extrapolation of laboratory rheological data, Tectonophysics, 133, 33–43, https://doi.org/10.1016/00401951(87)90278-2, 1987.

Paterson, M. and Luan, F. C.: Quartzite rheology under geological conditions, Geological Society, London, Special Publications, 54, 299 LP – 307, https://doi.org/10.1144/GSL.SP.1990.054.01.26, 1990.

Pfiffner, O. and Ramsay, J.: Constraints on geological strain rates: Arguments from finite strain states of naturally deformed rocks, Journal of Geophysical Research, 87, 311–321, https://doi.org/10.1029/JB087iB01p00311, 1982.

Plümper, O. and Putnis, A.: The Complex Hydrothermal History of Granitic Rocks: Multiple Feldspar Replacement Reactions under Subsolidus Conditions, Journal of Petrology, 50, 967–987, https://doi.org/10.1093/petrology/egp028, 2009.

Poirier, J.-P.: Creep of Crystals: High-Temperature Deformation Processes in Metals, Ceramics and Minerals, Cambridge Earth ~~Science Series~~ScienceSeries, Cambridge University Press, https://doi.org/10.1017/CBO9780511564451, 1985.

Prior, D. J. and Wheeler, J.: Feldspar fabrics in a greenschist facies albite-rich mylonite from electron backscatter diffraction, Tectonophysics,——303, 29–49, https://doi.org/10.1016/S0040-1951(98)00257-1, 1999.

Putnis, A.: Mineral Replacement Reactions, Reviews in Mineralogy and Geochemistry, 70, 87–124, https://doi.org/10.2138/rmg.2009.70.3, 2009.

Ratschbacher, L., Merle, O., Davy, P., and Cobbold, P.: Lateral extrusion in the eastern Alps, Part 1: Boundary conditions and experiments scaled for gravity, Tectonics, 10, 245–256, https://doi.org/10.1029/90TC02622, 1991.

Ree, J.-H., Kim, H. S., Han, R., and Jung, H.: Grain-size reduction of feldspars by fracturing and neocrystallization in a low-grade granitic mylonite and its rheological effect, Tectonophysics, 407, 227–237, https://doi.org/10.1016/j.tecto.2005.07.010, 2005.

Rosenberg, C. L. and Stünitz, H.: Deformation and recrystallization of plagioclase along a temperature gradient : an example from the Bergell tonalite, Journal of Structural Geology, 25, 389 – 408, https://doi.org/10.1016/S0191-8141(02)00036-6, 2003.

Rutter, E. H. and Brodie, K.: Lithosphere rheology – a note of caution, Journal of Structural Geology, 13, 363–367, https://doi.org/10.1016/0191-8141(91)90136-7, 1991.

Rybacki, E. and Dresen, G.: Deformation mechanism maps for feldspar rocks, Tectonophysics, 382, 173–187, https://doi.org/10.1016/j.tecto.2004.01.006, 2004.

Schmid, S. M., Fügenschuh, B., Kissling, E., and Schuster, R.: Tectonic map and overall architecture of the Alpine orogen, Eclogae Geologicae Helvetiae, 97, 93–117, https://doi.org/10.1007/s00015-004-1113-x, 2004.

Schulz, B.: Jungalpidische Gefügeentwicklung entlang der Defereggen-Antholz-Vals-Linie (Osttirol, Österreich), Jahrbuch der geologischen Bundesanstalt, 132, 775–789, 1989.

Schulz, B.: Microstructural Evolution of Metapelites from the Austroalpine Basement North of Staller Sattel During Pre-Alpine and Alpine Deformation and Metamorphism (Eastern Tyrol, Austria), Jahrbuch der geologischen Bundesanstalt, 137, 197–212, 1994.

Schulz, B., Steenken, A., and Siegesmund, S.: Geodynamic evolution of an Alpine terrane - the Austroalpine basement to the south of the Tauern Window as a part of the Adriatic Plate (eastern Alps), Geological Society London, Special Publications, 298, 5–44, https://doi.org/10.1144/SP298.2, 2008.

Schuster, R. and Stüwe, K.: Permian metamorphic event in the Alps, Geology, 36, 603, https://doi.org/10.1130/G24703A.1, 2008.

Simpson, C. and Wintsch, R.: Evidence for deformation-induced K-feldspar replacement by myrmekite, Journal of Metamorphic Geology, 7, 261–275, https://doi.org/10.1111/j.1525-1314.1989.tb00588.x, 1989.

Sinha, S., Alsop, G. I., and Biswal, T.: The evolution and significance of microfracturing within feldspars in low-grade granitic mylonites: A case study from the Eastern Ghats Mobile Belt, India, Journal of Structural Geology, 32, 1417–1429, https://doi.org/10.1016/j.jsg.2010.07.006, 2010.

881 Steenken, A., Siegesmund, S., and Heinrichs, T.: The emplacement of the Rieserferner Pluton
882   (Eastern Alps, Tyrol): Contraints from field observations, magnetic fabrics and
883   microstructures, Journal of Structural Geology, 22, 1855–1873,
884   https://doi.org/10.1016/S01918141(00)00071-7, 2000.

885 Stipp, M., Stünitz, H., Heilbronner, R., and Schmid, S. M.: The eastern Tonale fault zone: a
886   'natural laboratory' for crystal plastic deformation of quartz over a temperature range from
887   250 to 700 °C, Journal of Structural Geology, 24, 1861–1884,
888   https://doi.org/10.1016/S01918141(02)00035-4, 2002.

889 Stöckhert, B.: Deformation und retrograde Metamorphose im Altkristallin S' des westlichen
890   Tauerfensters (Südtirol), Ph.D. thesis, Universität Erlangen-Nürnberg, 1982.

891 Stöckhert, B.: K-Ar determinations on muscovites and phengites from deformed pegmatites,
892   and the minimum age of Old Alpine deformation in the Austridic basement to the South of
893   the western Tauern Window (Ahrn valley, Southern Tyrol, Eastern Alps), Neues Jahrbuch
894   für Mineralogie / Abhandlungen, 150, 103 – 120, 1984.

895 Stöckhert, B.: Das Uttenheimer Pegmatit-Feld (Ostalpines Altkristallin, Südtirol) Genese und
896   alpine Überprägung, Erlanger geologische Abhandlungen, 114, 83 – 106, 1987.

897 Stöckhert, B., Brix, M. R., Kleinschrodt, R., Hurford, A. J., and Wirth, R.: Thermochronometry
898   and microstructures of quartz - a comparison with experimental flow laws and predictions
899   on the temperature of the brittle-plastic transition, Journal of Structural Geology, 21, 351–
900   369, https://doi.org/10.1016/S0191-8141(98)00114-X, 1999.

901 Stünitz, H.: Syndeformational recrystallization - dynamic or compositionally induced?,
902   Contributions to Mineralogy and Petrology, 131, 219–236,
903   https://doi.org/10.1007/s004100050390, 1998.

904 Stünitz, H. and Fitz Gerald, J.: Deformation of granitoids at low metamorphic grade. II:
905   Granular flow in albite-rich mylonites, ~~Tectono physics~~Tectonophysics, 221, 299 – 324,
906   https://doi.org/10.1016/0040-1951(93)90164-F, 1993.

907 Stünitz, H., Fitz Gerald, J., and Tullis, J.: Dislocation generation, slip systems, and dynamic
908   recrystallization in experimentally deformed plagioclase single crystals, Tectonophysics,
909   372, 215–233, https://doi.org/10.1016/S0040-1951(03)00241-5, 2003.

910 Thöni, M. and Miller, C.: Garnet Sm-Nd data from the Saualpe and the Koralpe (Eastern Alps,
911   Austria): Chronological and P-T constraints on the thermal and tectonic history, Journal of
912   Metamorphic Geology, 14, 453–466, https://doi.org/10.1046/j.1525-1314.1996.05995.x,
913   1996.

914 Thöni, M. and Miller, C.: The "Permian event" in the Eastern European Alps: Sm–Nd and P–
915   T data recorded by multi-stage garnet from the Plankogel unit, Chemical Geology, 260, 20–
916   36, https://doi.org/10.1016/j.chemgeo.2008.11.017, 2009.

917 Trepmann, C. A., Stöckhert, B., and Chakraborty, S.: Oligocene trondhjemitic dikes in the
918   Austroalpine basement of the Pfunderer Berge, Südtirol – level of emplacement and
919   metamorphic overprint, European Journal of Mineralogy, 16, 641–659,
920   https://doi.org/10.1127/09351221/2004/0016-0641, 2004.

921 Tröger, W.: Optische Bestimmung der gesteinsbildenden Minerale. Teil I:
922   Bestimmungstabellen, Schweizerbart'sche Verlagsbuchhandlung, 5. edn.,
923   https://doi.org/10.1002/crat.2170180211, 1982.

924 Tsurumi, J., Hosonuma, H., and Kanagawa, K.: Strain localization due to a positive feedback
925   of deformation and myrmekite-forming reaction in granite and aplite mylonites along the

926   Hatagawa Shear Zone of NE Japan, Journal of Structural Geology, 25, 557–574,
927   https://doi.org/10.1016/S0191-8141(02)00048-2, 2003.

928 Tullis, T, E. and Tullis, J.: Experimental Rock Deformation Techniques, pp. 297–324 American
929   Geophysical Union, https://doi.org/10.1029/GM036p0297, 1986.

930 Tullis, J.: Deformation of Feldspars, in: Reviews in Mineralogy: Feldspar Mineralogy, edited
931   by Ribbe, P. H., chap. 13, pp. 297–323, The Mineralogical Society of America, 1983.

932 Tullis, J. and Yund, R. A.: Dynamic recrystallization of feldspar : A mechanism for ductile
933   shear   zone   formation,   Geology,   13,   238–241,   https://doi.org/10.1130/0091-
934   7613(1985)13<238:DROFAM>2.0.CO;2, 1985.

935 Tullis, J. and Yund, R. A.: Transition from cataclastic flow to dislocation creep of feldspar :
936   Mechanisms and microstructures, Geology, 15, 606–609, https://doi.org/10.1130/0091-
937   7613(1987)15<606:TFCFTD>2.0.CO;2, 1987.

938 Tullis, J. and Yund, R. A.: The Brittle-Ductile Transition In Feldspar Aggregates : An
939   Experimental Study, International Geophysics, 51, 89 –   117,
940   https://doi.org/10.1016/S0074-6142(08)62816-8, 1992.

941 Tullis, J., Yund, R. A., and Farver, J.: Deformation-enhanced fluid distribution in feldspar
942   aggregates   and   implications   for   ductile   shear   zones,   Geology,   24,   63–66,
943   https://doi.org/10.1130/0091-7613(1996)024<0063:DEFDIF>2.3.CO;2, 1996.

944 Voll, G.: Recrystallization of Quartz, Biotite and Feldspars from Erstfeld to the Leventina
945   Nappe, Swiss Alps, and its Geological Significance, Schweizerische mineralogische und
946   petrographische Mitteilungen, 56, 641–647, 1976.

947 Wassmann, S., Stöckhert, B., 2013. Rheology of the plate interfaced - dissolution precipitation
948   creep in high pressure metamorphic rocks. Tectonophysics 608, 1-29.

949 Wheeler J., Mariani, E., Piazolo, S.; Prior, D.J., Trimby, P., Drury, M.R., 2009. The weighted
950   Burgers vector: a new quantity for constraining dislocation densities and types using
951   electronbackscatter diffraction on 2D sections through crystalline materials. Journal of
952   Microscopy,Vol.233, Pt32009, pp.482–494.

953 White, S.: Tectonic deformation and recrystallisation of Oligoclase, Contributions to
954   Mineralogy and Petrology, 50, 287–304, https://doi.org/10.1007/BF00394854, 1975.

955 Yund, R. A.: Interdiffusion of NaSi-CaAl in peristerite, Physics and Chemistry of Minerals, 13,
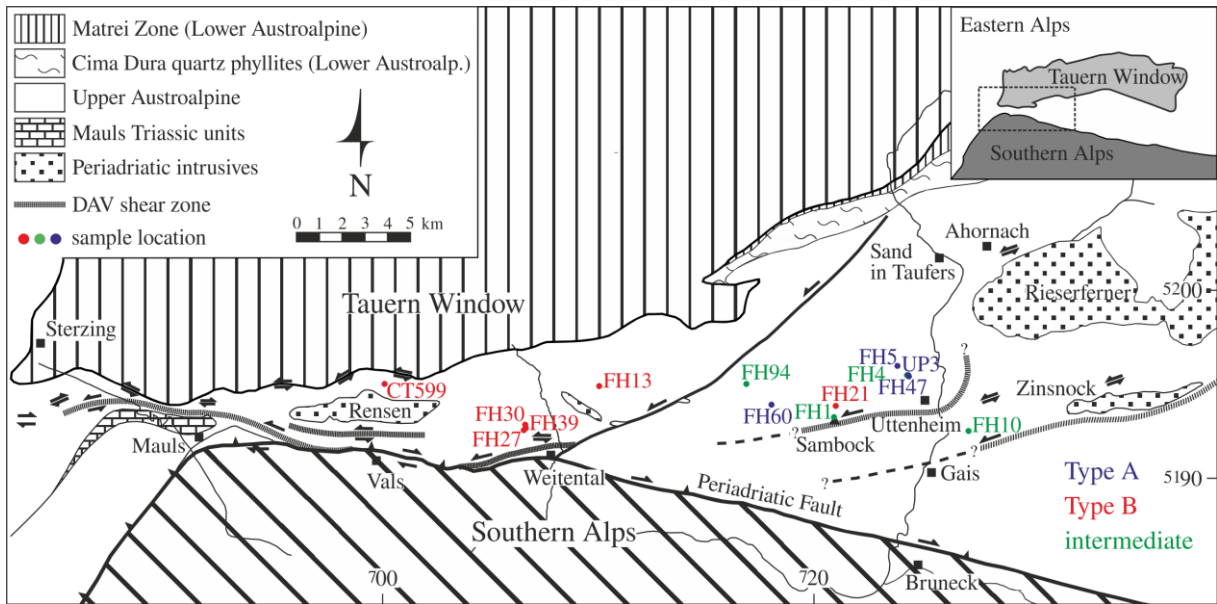956   11–16, https://doi.org/10.1007/BF00307308, 1986.

957

Fig. 1: Geologic map of the study area (modified after Mancktelow et al., 2001). The sample numbers are colored according to the type of albite-quartz matrix (see text and Table 1)
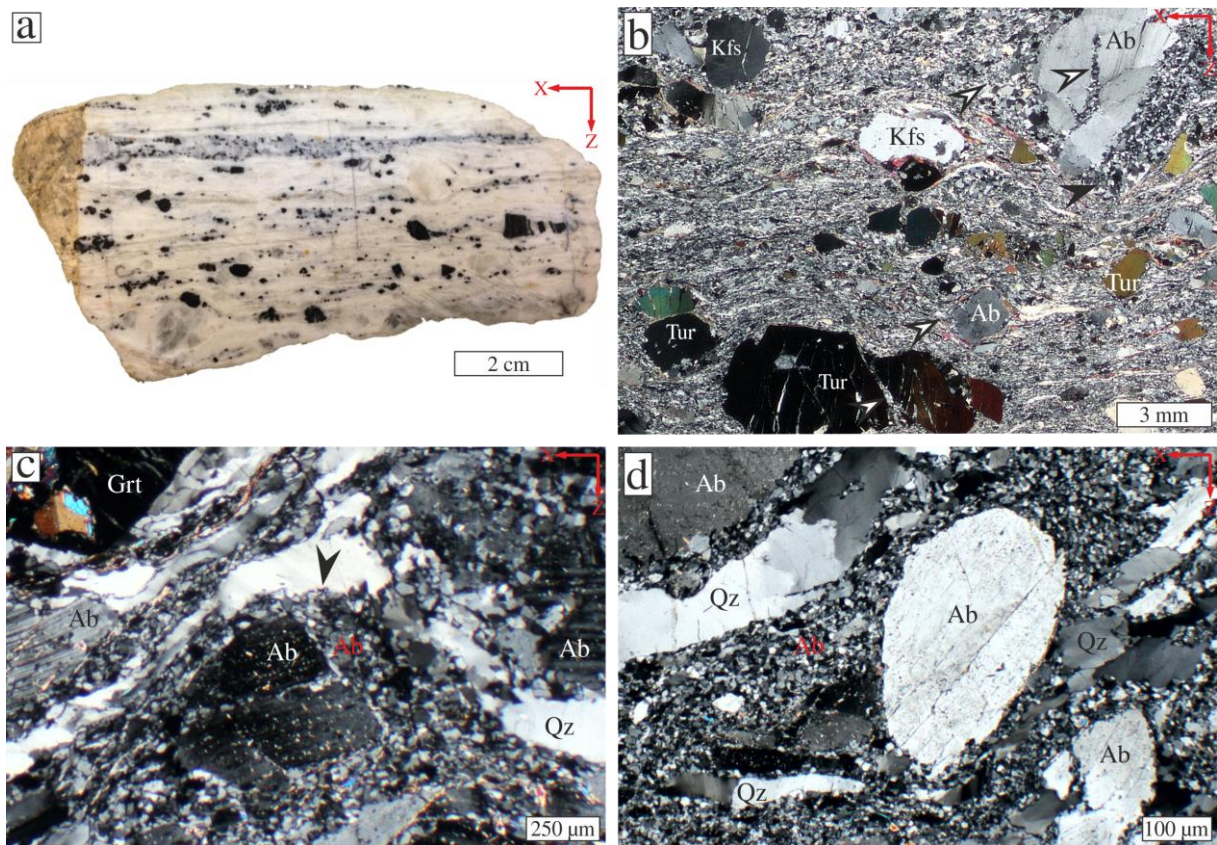

Fig. 2: Photograph of polished surface **(a)** and thin section micrograph taken with crossed polarizers **(b)** of sample CT599. K-feldspar (Kfs), albite (Pl) and tourmaline (Tur) porphyroclasts are embedded in a fine-grained matrix. Elongate fractured tourmaline crystals are oriented with their long axes parallel to the stretching lineation (x). Fractures are commonly oriented at low angle to the shortening direction (z). Arrows point to strain shadows surrounding porphyroclast and prismatic strain shadows between fragments of tourmaline and feldspar. Black arrow points to mylonitic foliation flowing around strain shadow. **(c, d)** Polarized light micrographs (crossed polarizers, sample FH5b) showing mylonitic foliation defined by quartz layers (Qz) flowing around garnet (Grt) and albite porphyroclasts (Pl), which are partly disintegrated into a fine-grained albite matrix.
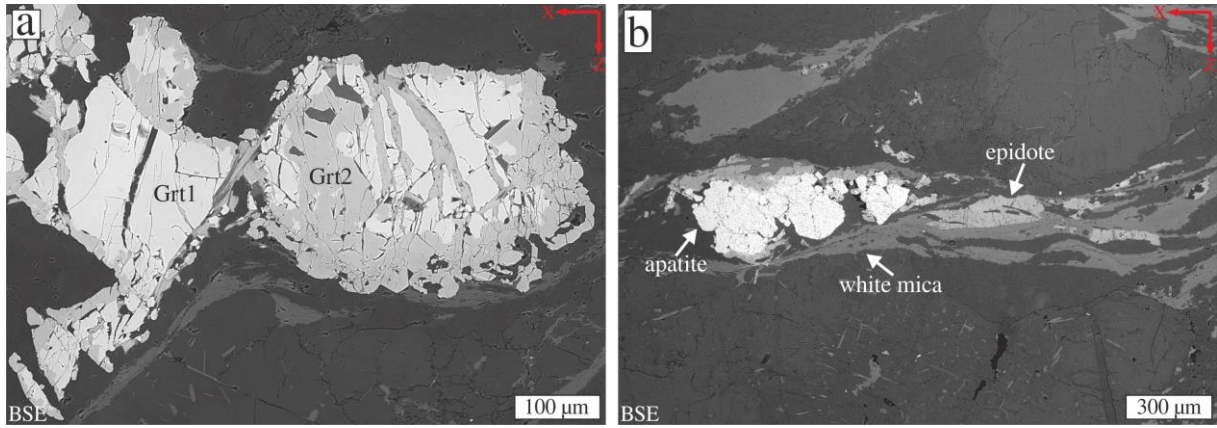
Fig. 3: BSE images from sample FH27 showing the typical accessory mineral assemblage in the deformed pegmatites: **(a)** Ca-rich garnet (Grt2) replacing magmatic Fe-rich garnet (Grt1). **(b)** Epidote and white mica aligned in the foliation with apatite porphyroclasts.
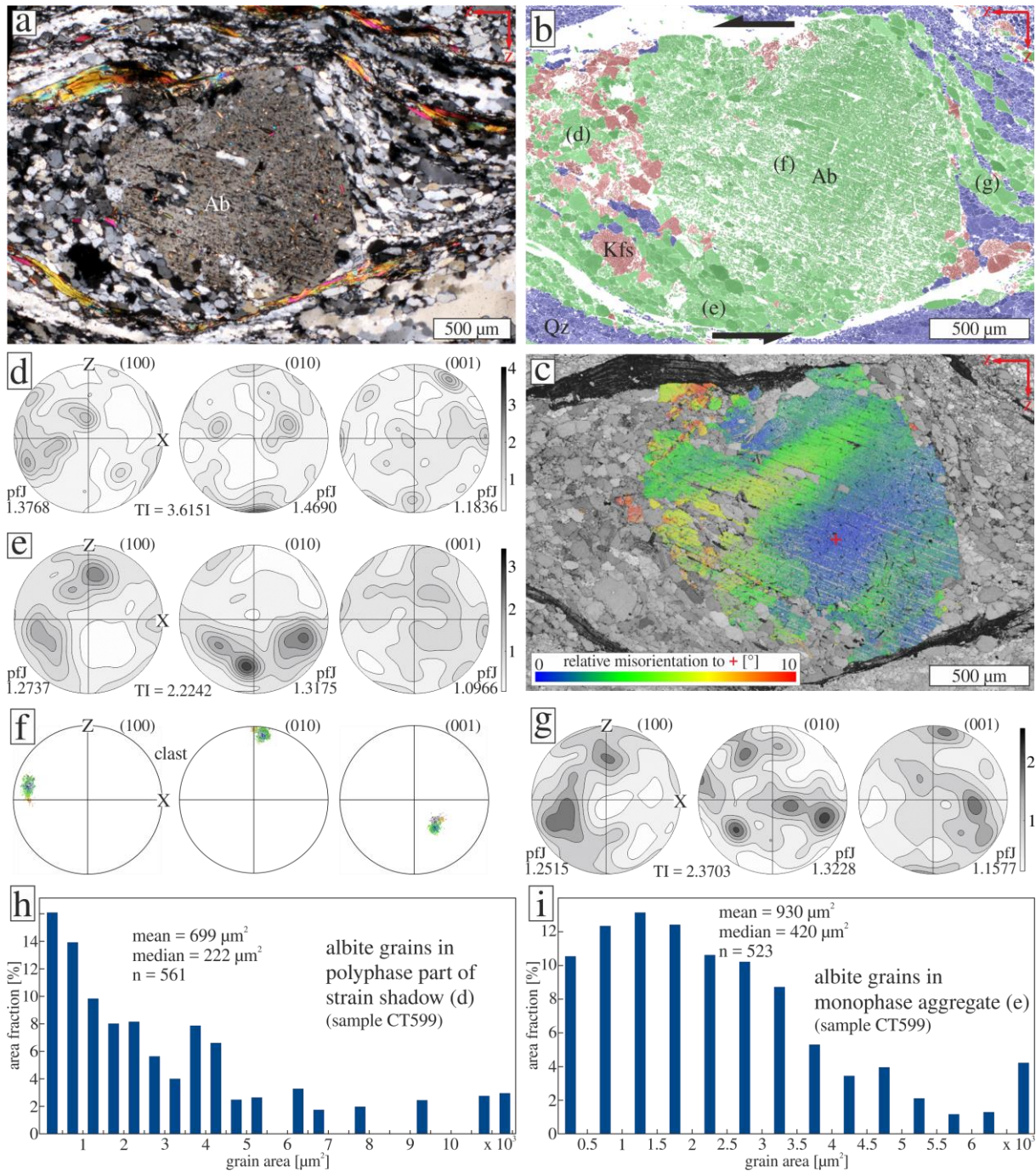
Fig. 4: **(a)** Asymmetric strain shadow around albite porphyroclast in sample CT599 in thin section micrograph with crossed polarizers**. (b)** EBSD-phase map of the same area (quartz: blue, albite: green, K-feldspar: red) and **(c)** EBSD-relative misorientation map (0-10°) of the albite porphyroclast. Polyphase aggregates occur mostly in the upper left and lower right of the clast. In the other quadrants monophase albite dominates. Pole figures show the orientation of albite in the strain shadow in the upper left quadrant **(d)**, lower left quadrant **(e)**, albite porphyroclast **(f)** and in the upper right quadrant **(g)**. Grain ~~size~~ area distribution histograms of albite in polyphase aggregates strain shadow **(h)** and in monophase albite aggregates **(i)**.
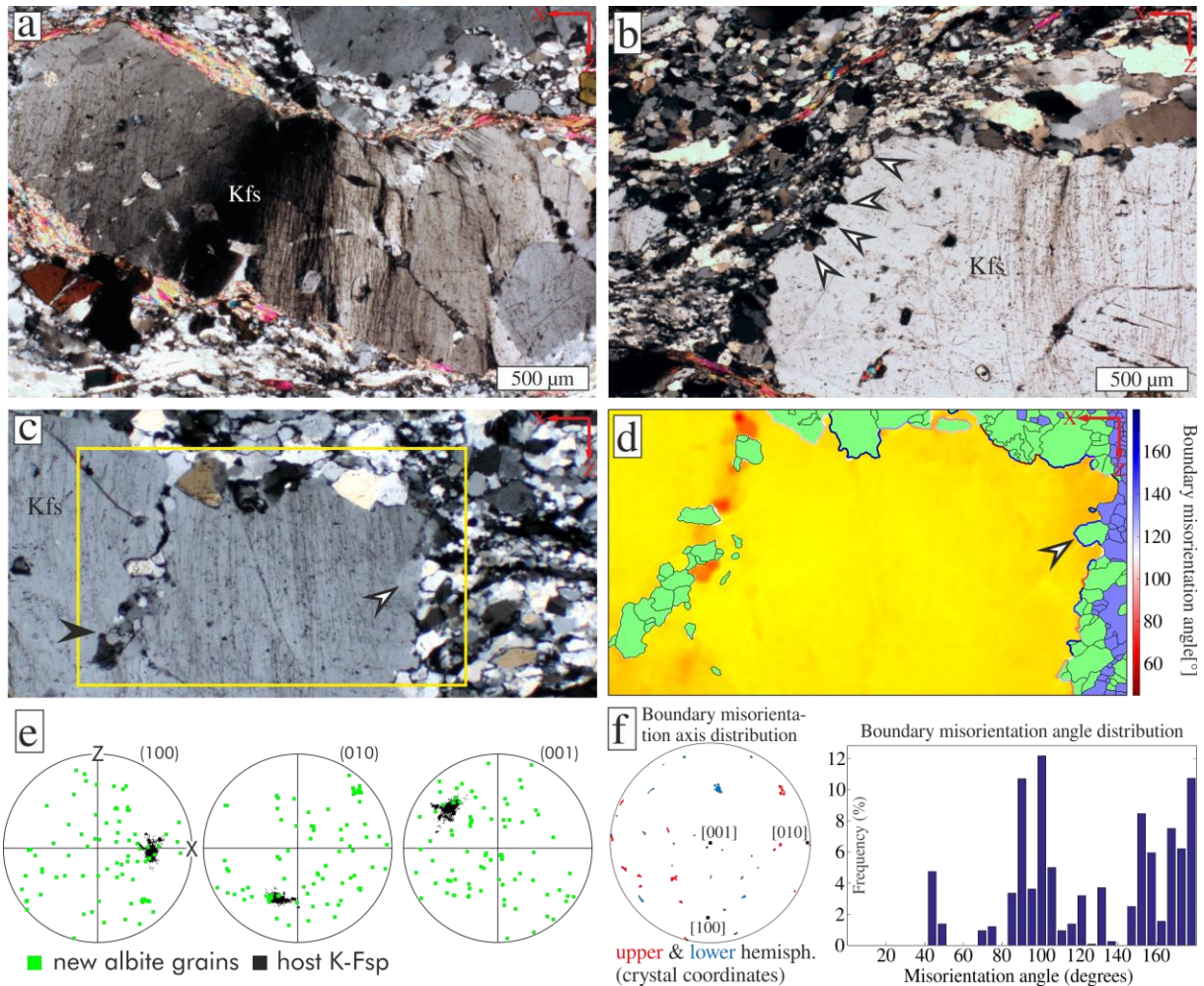
Fig. 5: K-feldspar deformation microstructures (sample CT599). **(a, b)** Polarized light micrographs (crossed polarizers) of bent K-feldspar porphyroclast with healed microcracks parallel to the shortening direction and ~~sawtooth-shaped~~cuspate grain boundaries (white arrows in (b)). **(c, ~~d~~)** Polarized light micrograph (crossed polarizers) showing K-feldspar with fractures filled with albite (black arrow) and cuspate phase boundaries. Healed microcracks are cut-off by newly formed albite (white arrow). Yellow rectangle shows area of EBSD map in (d). **(d)** EBSD map, where boundaries between replacing albite grains (green) and the K-feldspar-host (yellow) are colored after their misorientation angle. Quartz in the matrix is blue in color. **(e)** Polefigures of poles to (100), (010) and (001) planes of new albite grains (green) and K-feldspar porphyroclast (black). **(f)** Misorientation angle and axis distribution for the boundaries colored in (d).~~and corresponding EBSD map (yellow rectangle in (c)) showing K-feldspar with fractures filled with albite and K-feldspar (black arrows) and sawtooth-shaped phase boundaries. Numbers in the EBSD map indicate the misorientation angles between new grain and host, which are generally high. The colour coding of the porphyroclast is by relative misorientation angle of 7° from yellow to black. (e) Pole figures for albite grains replacing K-feldspar porphyroclast along its rim show, that there is no relationship between the new albite grains and the Kfs-host.~~
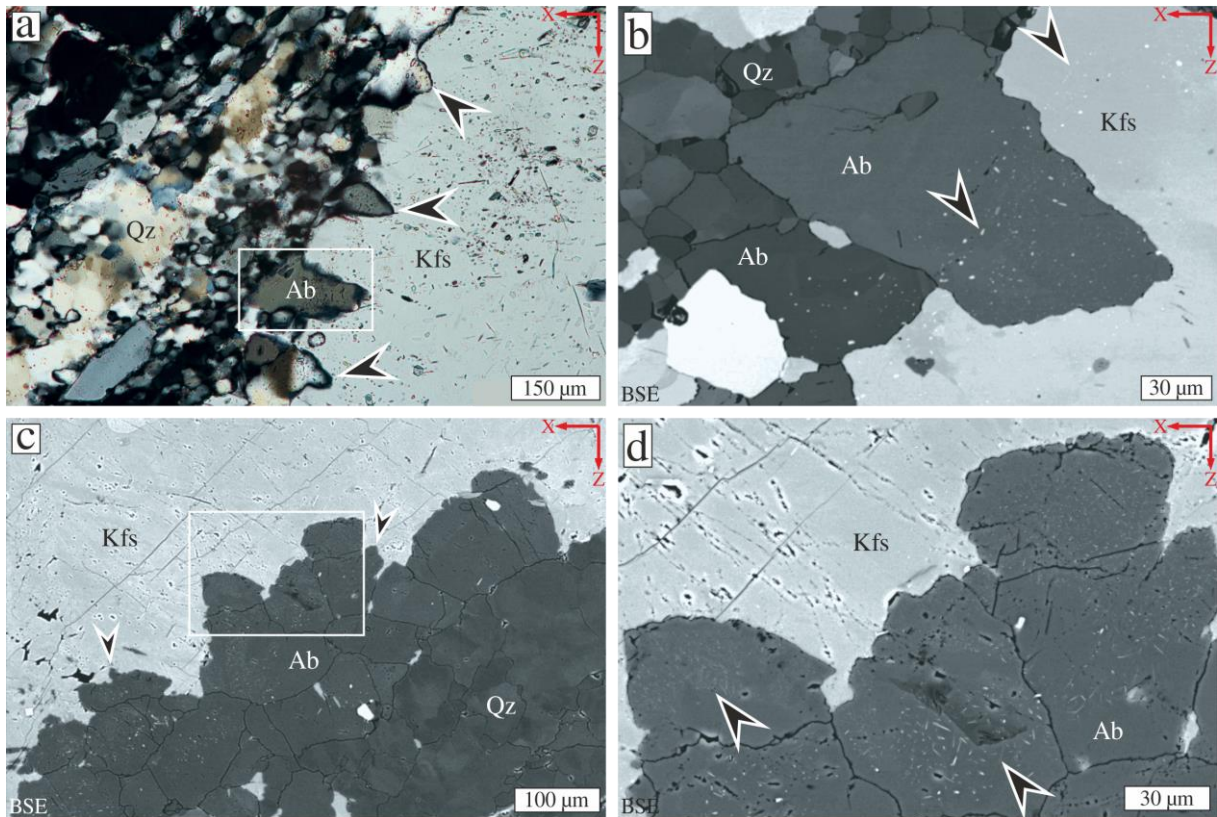
Fig. 6: (a) Photomicrograph of ~~sawtooth shaped~~cuspate interface between K-feldspar clast and new albite grains (sample CT599). (**b**) Close-up BSE-image of location indicated by white box in (a). Note the tiny apatite inclusions in the albite (determined by EDS, arrows). (**c**) BSE-image of ~~sawtooth shaped~~cuspate interface between albite replacing K-feldspar in sample FH14. The arrows point to protrusions. (**d**) Close-up BSE-image of white box in (c) showing the numerous tiny (< 5 µm) apatite inclusions in the replacing albite.
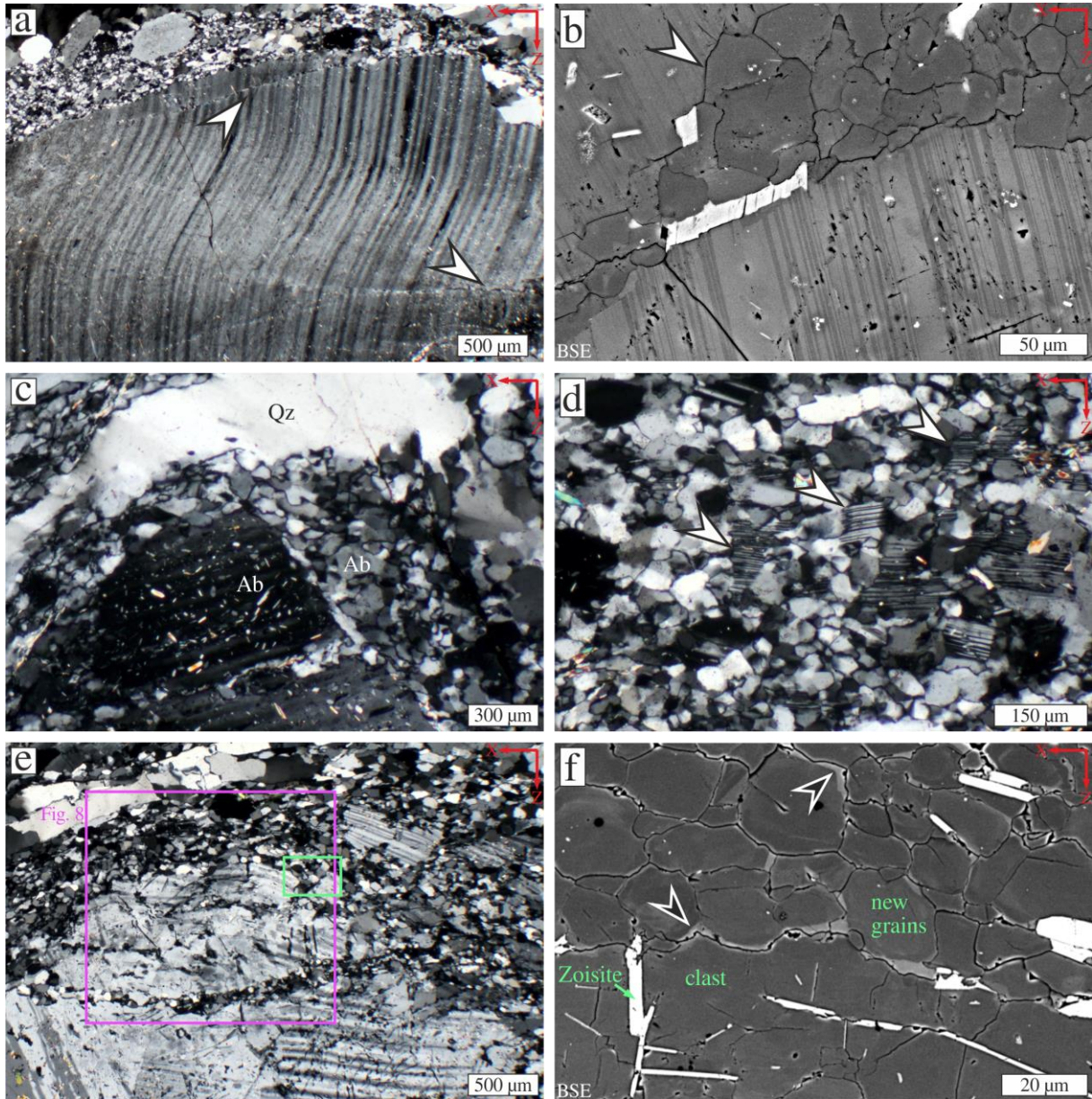
Fig. 7: **(a)** Polarized light micrograph (crossed polarizers) and **(b)** BSE image of bent and kinked twins in albite porphyroclast, sample FH5. New albite grains occur along fractures parallel to kink band boundaries (arrows). **(c)** Polarized light micrograph (crossed polarizers), showing fragmented albite porphyroclast partly replaced by new grains and surrounded by quartz layer, sample FH5. **(d)** Polarized light micrograph (crossed polarizers) showing twinned albite fragments surrounded by fine-grained albite matrix, sample FH5. **(e)** Polarized light micrograph (crossed polarizers) of twinned and fractured albite porphyroclast, sample UP3. Green box indicates area of BSE image in (f), violet box indicates EBSD map shown in Fig 8. **(f)** BSE image showing new albite grains adjacent to the albite porphyroclast. New grains often have an outer rim of less albitic plagioclase, up to An_{20} (arrows). The bright phase are zoisite needles.
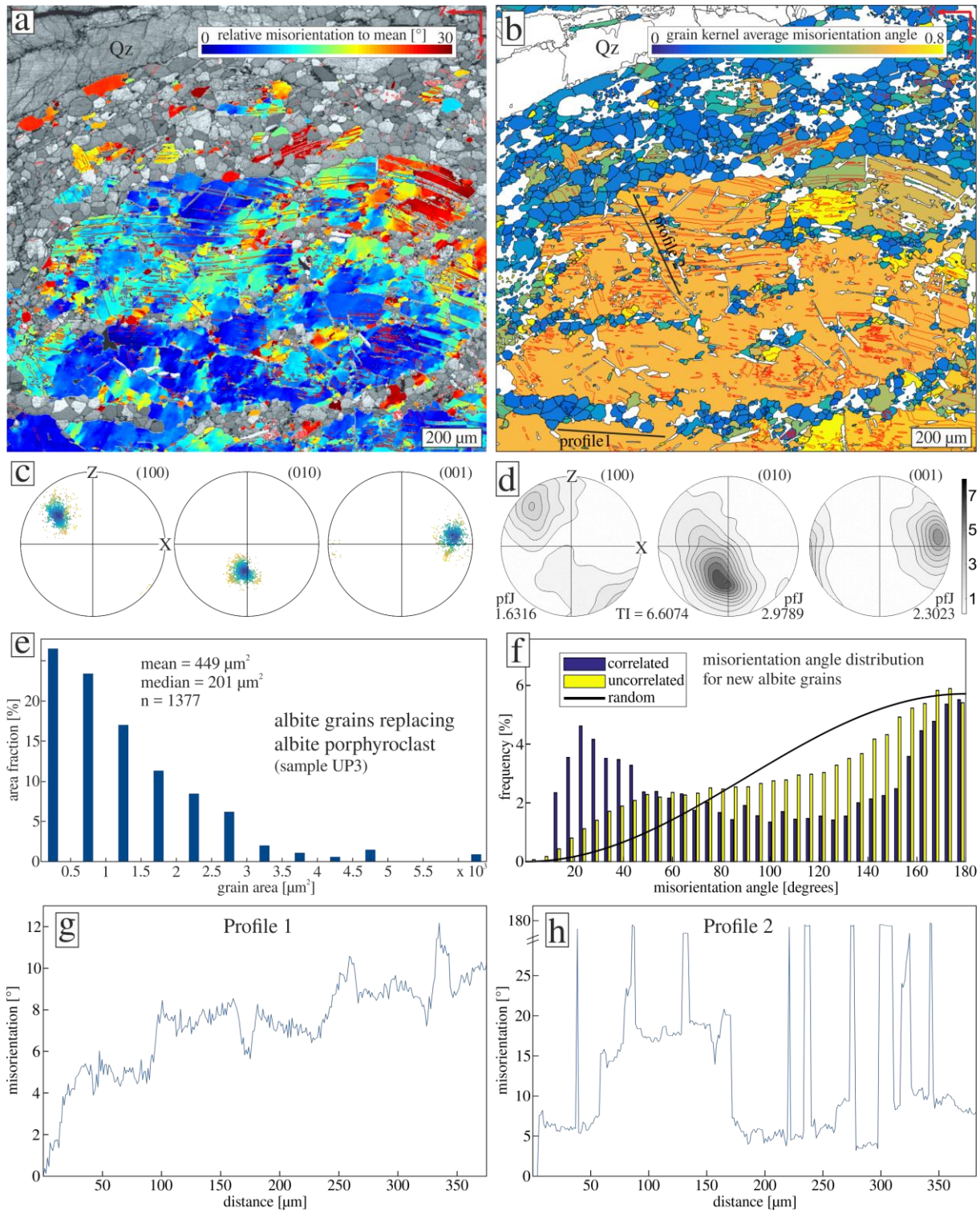
Fig. 8: **(a, b)** EBSD-relative misorientation map for albite relative to the mean orientation of the porphyroclast **(a)** and grain kernel average misorientation (gKAM)-map, showing a lower inferred dislocation density for new grains **(b)** of the area in the violet box in Fig. 7b. Red lines in are albite and pericline twin boundaries. **(c, d)** Corresponding pole figures colour coded corresponding to EBSD-relative misorientation map **(c)** and scatter plot (color-coded corresponding to (a)), where only grains smaller than 100 µm and free of visible twins were used. **(e)** Grain area distribution for new grains smaller than 100 µm. **(f)** Misorientation angle distribution for adjacent and random pairs of new albite grains. **(g, h)** Misorientation profiles (relative to origin) along lines shown in (b). ~~EBSD-relative misorientation map (a) and grain kernel average misorientation (gKAM)-map, showing a lower inferred dislocation density for new grains (b) of the area in the violet box in Fig. 7b. Red lines in (a) are low angle grain boundaries of 3-10° misorientation. **(c, d)** Corresponding pole figures colour coded corresponding to EBSD-relative misorientation map (c) and scatter plot, where only grains smaller than 100 µm and free of visible twins were used. **(e)** Grain size distribution for new grains smaller than 100 µm. **(f)** Misorientation angle distribution for adjacent and random pairs of new albite grains. **(g, h)** Misorientation profiles along lines shown in (b).~~
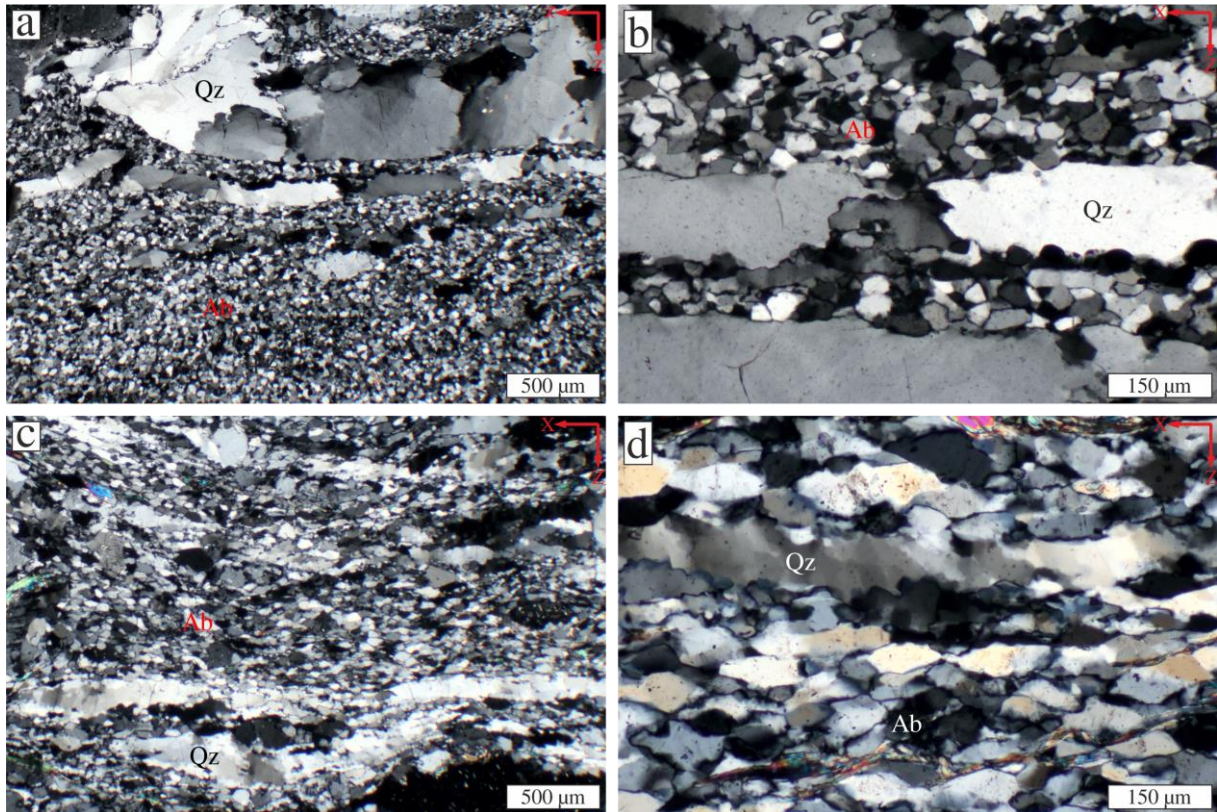
Fig. 9: Polarized light micrographs taken with crossed polarizers showing the two types of quartz-albite matrix microstructure. **(a, b)** Type A matrix is characterized by coarse quartz layers and albite layers with isometric small grains, sample FH5. **(c, d)** Type B matrix is characterized by albite layers characterized by coarser and elongate grains parallel to the foliation, and fine-grained, dynamically recrystallized quartz layers, samples CT599.
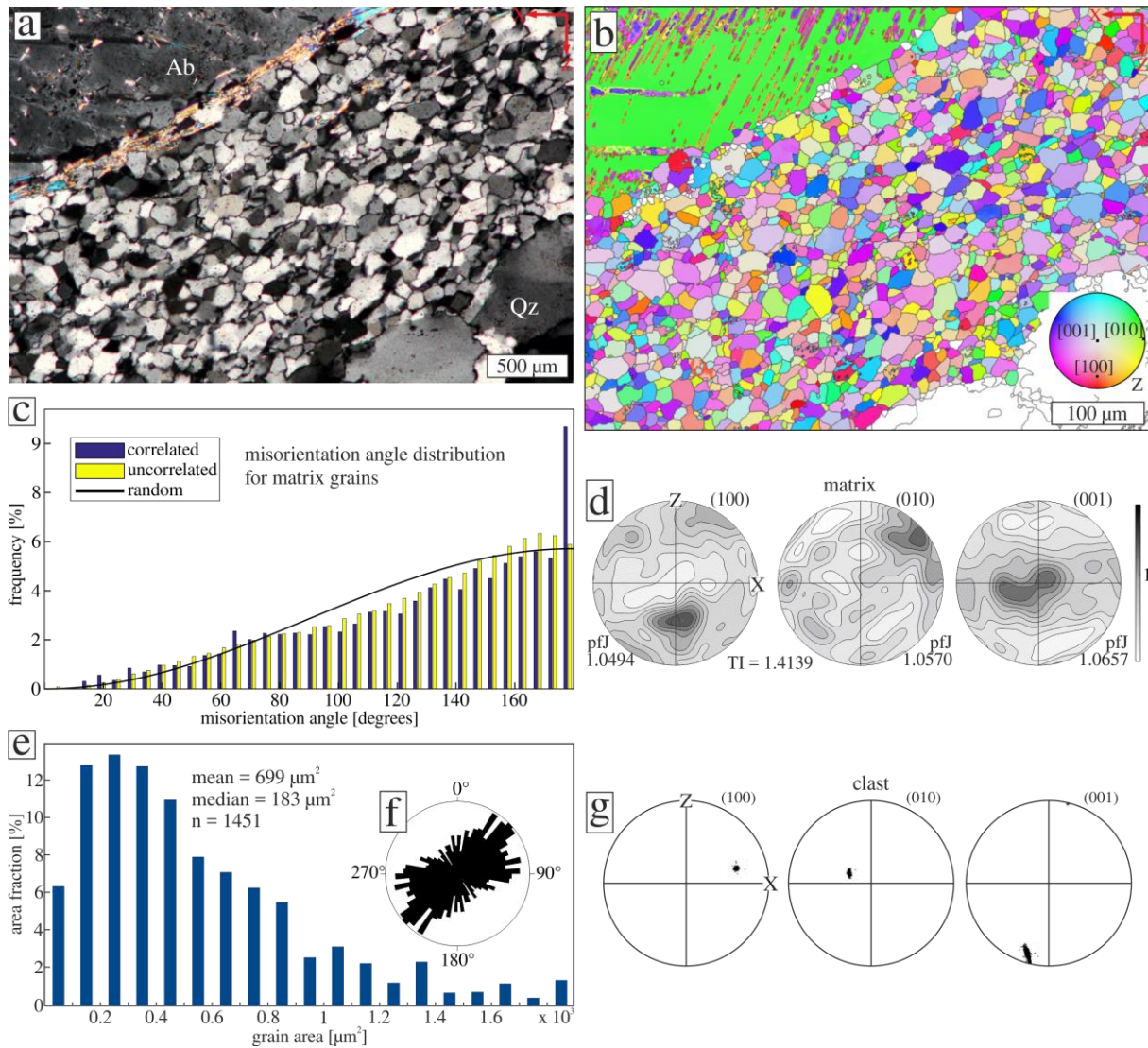
Fig. 10: EBSD-analysis of type A albite matrix in sample FH5. **(a)** Photomicrograph of the analysed area. **(b)** EBSD-map with inverse pole figure colouring (see lower inset). ~~Albite t~~Twin boundaries in the porphyroclast are shown as red lines. **(c)** Misorientation angle distribution showing an essentially random distribution of neighbouring or random grain pairs. **(d)** Contoured pole figures showing orientation distribution of albite matrix grains. ~~Maximum mud = 3.1.~~ **(e)** Grain ~~size~~ area distribution of the measured matrix grains. **(f)** Rose diagram showing the orientation of the long axis of grains. **(g)** Pole figures showing the orientation of the albite porphyroclast from (a, b).
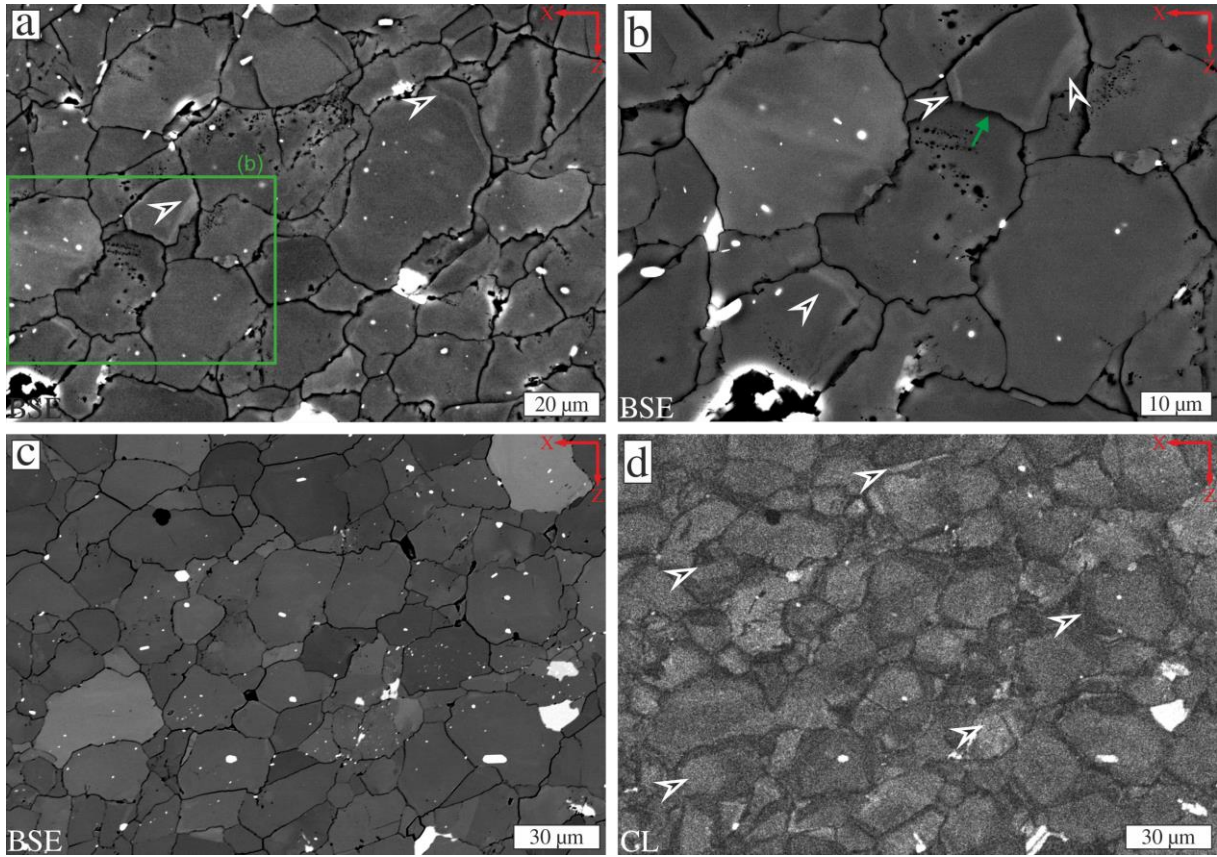
Fig. 11: Type A matrix, sample FH5. **(a, b)** BSE images show albite matrix with irregular grain boundaries, porosity and weak zonation (black arrows). In (b), the zonation of the grain in the upper right is truncated, possibly by growth of the grain below (green arrow). **(c)** BSE image with grey shades representing both, orientation and compositional contrast (bright phase is apatite) and **(d)** corresponding CL image showing zonations, not visible in the BSE image (arrows). Grain boundaries in the CL image are also associated to darker grey shades.
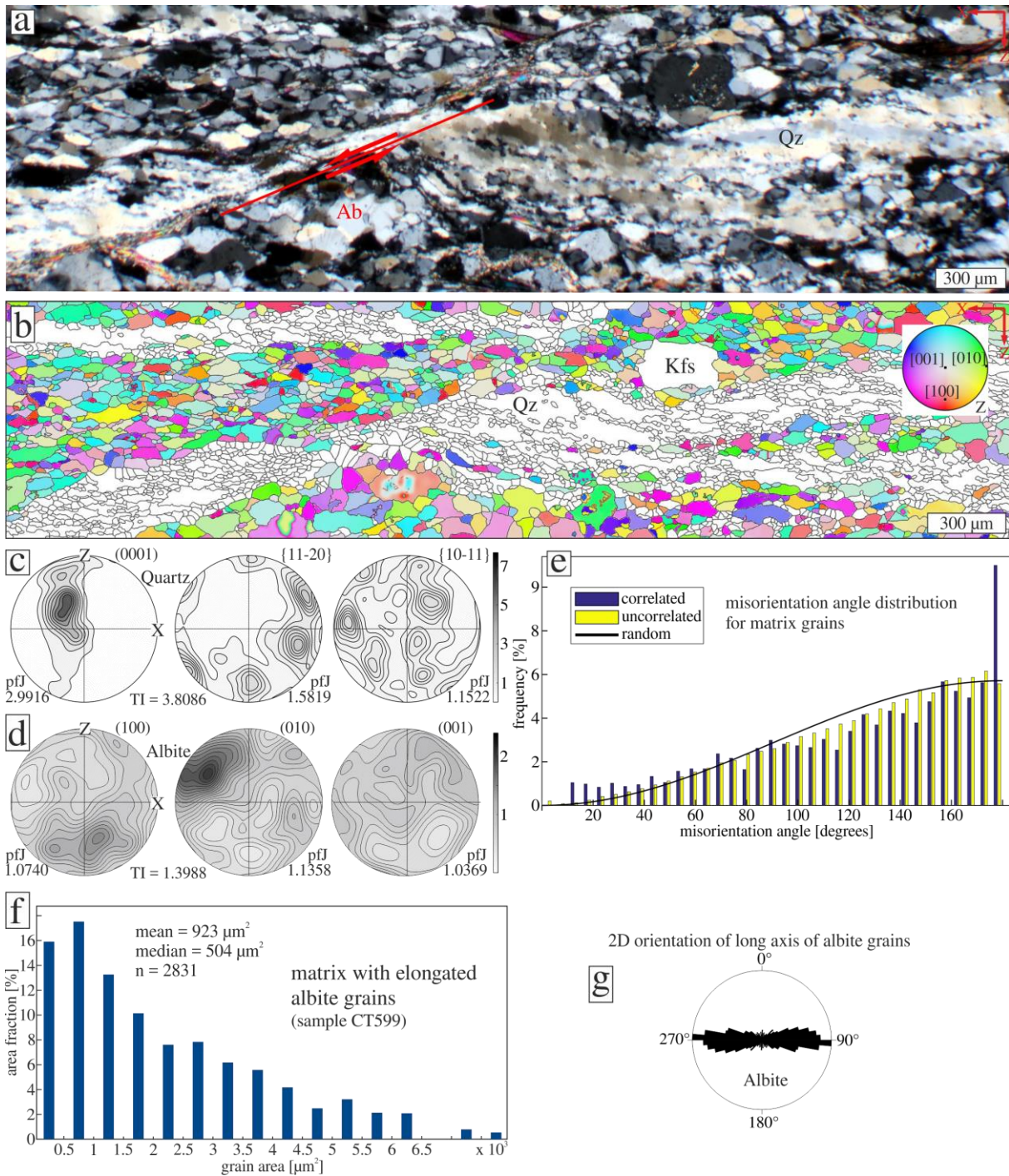
Fig. 12: **(a)** Photomicrograph of the type B matrix with coarse monophase albite and fine-grained quartz layers in sample CT599. Quartz and albite layers are offset at the shear band marked red. **(b)** EBSD-map of the area from (a) with an IPF colour code (Z-axis). Only albite is coloured after the IPF-colour-code. **(c)** Pole figures for albite grains from (db). ~~Maximum mud = 3.3.~~ **(d)** Pole figures for quartz grains from (db). ~~Maximum mud = 7.9.~~ **(e)** Misorientation angle distribution showing an essentially random distribution of neighbouring or random grain pairs. **(f)** Grain ~~sized~~ area distribution diagram**. (g)** Rose diagram of the long axis of albite matrix grains from the area measured by EBSD.
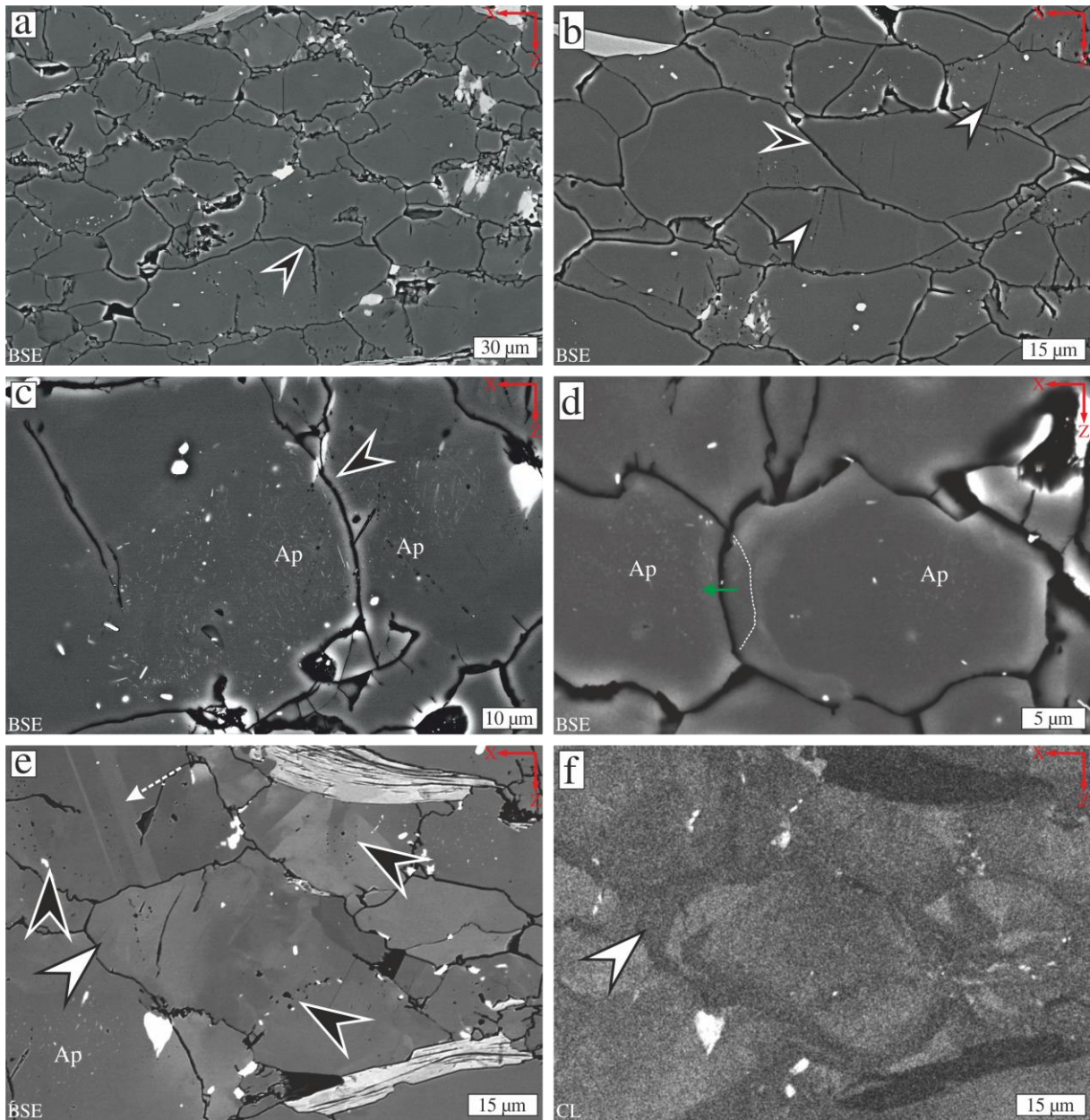
Fig. 13: BSE images of albite grains in type B matrix. **(a)** Overview showing elongate albite grains and some relict Kfs grains (light grey). Note grain boundary affected by a crack in the grain below (arrow). **(b)** Boundaries can be remarkably straight, especially at low angle to the foliation (black arrow). Healed microcracks at low angle to shortening direction are indicated by increased porosity (white arrows). **(c)** Apatite needles in albite grains. Apatite rich zone is crosscut by grain boundary (arrow). **(d)** Albite grains showing Ca-enriched zone, representing growth rim (green arrow represents growth direction) with the former grain boundary preserved by the zonation (dashed line). **(e)** Grain with twins (dashed arrow). Black arrows point to porosity, which is associated with zonation (white arrow), best seen in the CL image (f). The zonation is probably due to changing contents of trace elements, which cannot be resolved in the BSE image.
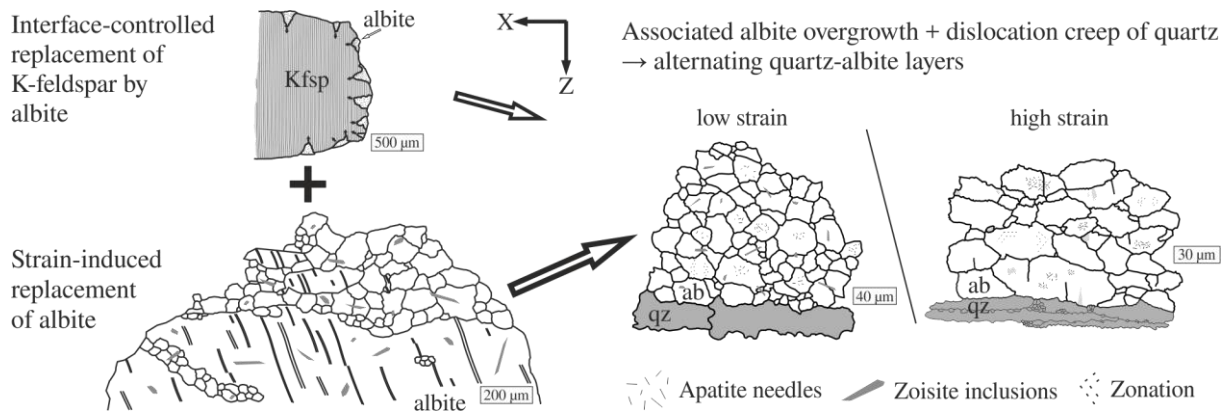
Fig. 14: Conceptual sketch of the formation of the mylonitic albite matrix. The contribution of replacement of albite porphyroclasts by albite is larger than that of replacement of K-feldspar (see text for discussion).